AGU100 ADVANCING EARTH AND SPACE SCIENCE

Tectonics

RESEARCH ARTICLE
10.1029/2018TC005073

Key Points:
- The Grant Range detachment system accommodated 24 km of extension (115%) between 31 and 15 Ma and was a significant syn-rollback fault system
- Decreased interplate coupling during slab rollback likely drove the earliest episode of distributed extension in the Cordilleran plateau
- Muscovite $^{40}Ar/^{39}Ar$ multi-diffusion domain modeling is effective for constraining the cooling histories of rocks between ~425 and 250 °C

Supporting Information:
- Supporting Information S1

Correspondence to:
S. P. Long,
sean.p.long@wsu.edu

Citation:
Long, S. P., Heizler, M. T., Thomson, S. N., Reiners, P. W., & Fryxell, J. E. (2018). Rapid Oligocene to early Miocene extension along the Grant Range detachment system, Nevada, USA: Insights from multipart cooling histories of footwall rocks. *Tectonics*, *37*, 4752–4779. https://doi.org/10.1029/2018TC005073

Received 26 MAR 2018
Accepted 12 OCT 2018
Accepted article online 15 OCT 2018
Published online 22 DEC 2018

Rapid Oligocene to Early Miocene Extension Along the Grant Range Detachment System, Nevada, USA: Insights From Multipart Cooling Histories of Footwall Rocks

Sean P. Long[1], Matthew T. Heizler[2], Stuart N. Thomson[3], Peter W. Reiners[3], and Joan E. Fryxell[4]

[1]School of the Environment, Washington State University, Pullman, WA, USA, [2]New Mexico Bureau of Geology and Mineral Resources, New Mexico Tech, Socorro, NM, USA, [3]Department of Geosciences, University of Arizona, Tucson, AZ, USA, [4]Department of Geological Sciences, California State University, San Bernardino, CA, USA

Abstract In Nevada and Utah, the Cordilleran orogen underwent a protracted Cenozoic transition to an extensional setting. However, the geodynamic processes that controlled this transition are poorly understood, in part because the space-time patterns of extension are not known in many areas. Localities of pre-Neogene extension have the potential to elucidate the dynamics of the Cordilleran crust during the final stages of subduction. Here we present data that constrain the timing of extension in the Grant Range in eastern Nevada, which was deformed by a low-angle normal fault system. We present temperature-time histories of eight granite samples exhumed by this fault system, constrained by muscovite $^{40}Ar/^{39}Ar$ multi-diffusion domain modeling and fission track and (U-Th)/He ages from zircon and apatite. These data demonstrate rapid cooling (20–35 °C/Myr) from 350–425 to 25–50 °C between 28–31 and 15–19 Ma. The fault system accommodated ~24 km of extension (~115%), and exhumed the granite samples from 7–9 km depths to the near-surface. Rapid Oligocene-early Miocene cooling is interpreted to date the duration of motion on the fault system, and defines an extension rate of 1.5–2.6 km/Myr. This was one of the most significant fault systems active during an episode of spatially distributed late Eocene-Oligocene extension, which overlaps temporally with volcanism generated by slab rollback. Reduced interplate coupling that accompanied slab rollback is interpreted as the primary driver of extension of the Cordilleran plateau during the final stages of subduction. This supports a scenario of orogenic collapse that proceeded in distinct episodes that were initiated by external geodynamic events.

1. Introduction

The processes that govern the extensional collapse of thickened orogenic crust have been the subject of long-standing debate (e.g., Allmendinger, 1992; Burchfiel & Royden, 1985; Coney & Harms, 1984; Dalmayrac & Molnar, 1981; Dewey, 1988; Dilek & Moores, 1999; Molnar & Lyon-Caen, 1988; Sonder & Jones, 1999), yet are critically important for understanding the full evolution of the orogenic cycle. The Cordilleran orogen in Nevada and Utah, which was constructed between the Jurassic and Paleogene as a result of Andean-style subduction (e.g., DeCelles, 2004), has undergone a complex and protracted history of Cenozoic extensional tectonism. The cumulative result has been construction of the Basin and Range Province, which formed dominantly from distributed Neogene extension following reorganization of the North American-Pacific plate boundary into a transform system (e.g., Atwater, 1970; Colgan & Henry, 2009; Dickinson, 1997, 2002; Faulds & Henry, 2008). However, due to the structural complexity of the province, the space-time patterns and driving mechanisms of extension remain debated. In particular, localities of pre-middle Miocene extension that predate what many interpret as the inception of widespread "Basin and Range" extension (e.g., Colgan et al., 2006; Colgan & Henry, 2009; Dickinson, 2002, 2006) remain intriguing, as they have the potential to elucidate the dynamics of the Cordillera during the final stages of subduction. Pre-Neogene extension in Nevada and Utah has been documented in a limited number of places, and has been attributed to orogenic wedge adjustment following Late Cretaceous lithospheric delamination (e.g., Druschke, Hanson, Wells, Rasbury, et al., 2009; Long et al., 2015; Wells & Hoisch, 2008; Wells et al., 2012), and to relaxation of interplate coupling during Eocene-Oligocene slab rollback and accompanying felsic magmatism (e.g., Dickinson, 2002; Gans et al., 1989, 2001; Humphreys, 1995).

One site of likely pre-middle Miocene extension is the Grant Range in east-central Nevada (Figure 1). The Grant Range is a core complex-type range that has undergone high-magnitude (~100%) extension

10.1029/2018TC005073

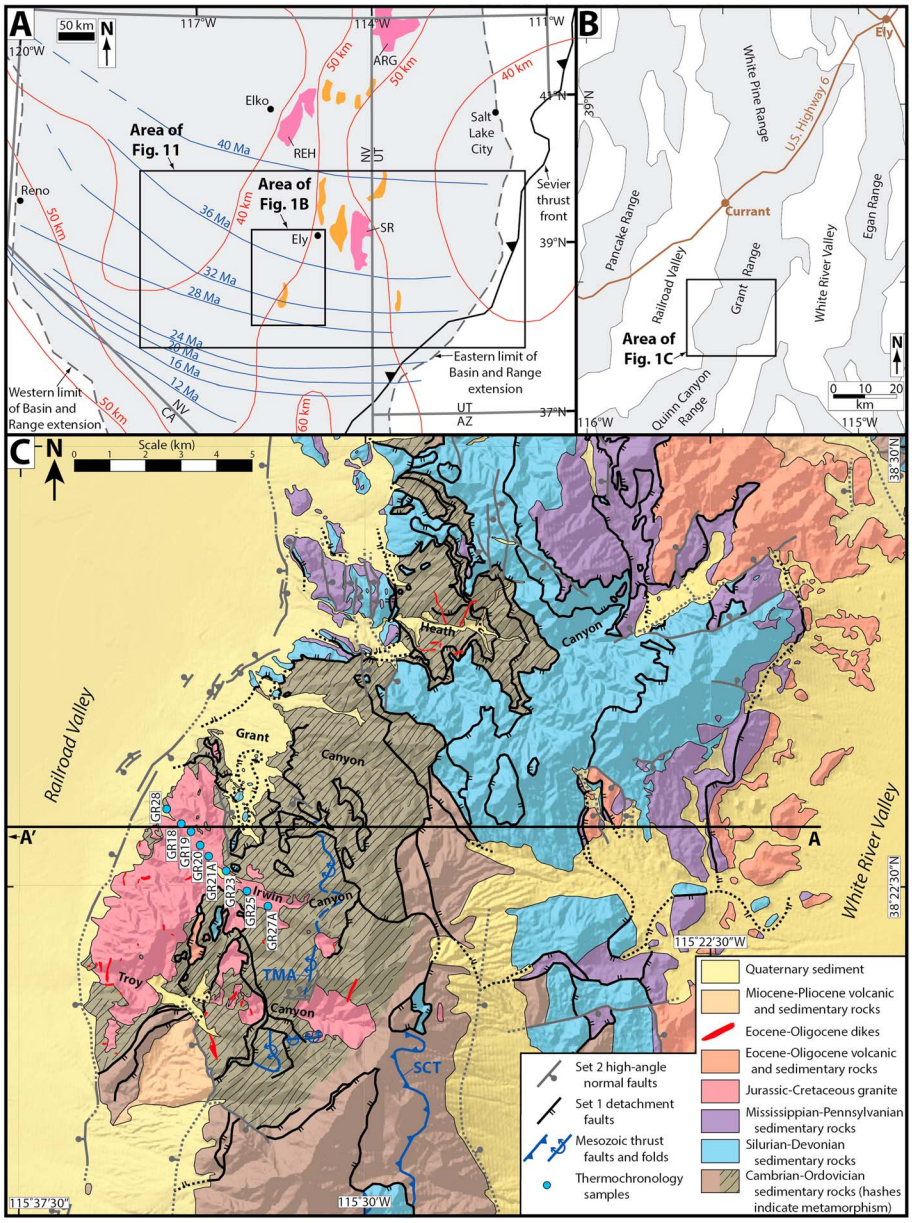

Figure 1. (a) Map of western Utah and Nevada (modified from Long & Walker, 2015); metamorphic core complexes are shown in pink, and exposures of Mesozoic metasedimentary rocks are shown in orange. Blue lines show age contours of initial ignimbrite flare-up magmatism (from Henry & John, 2013). Red lines show contours of estimated pre-extensional crustal thickness (from Best et al., 2009; Coney & Harms, 1984). Basin and Range Province boundaries are from Dickinson (2006). Abbreviations: SR = Snake Range core complex; REH = Ruby-East Humboldt core complex; ARG = Albion-Raft River-Grouse Creek core complex. (b) Map showing the Grant Range and names of proximal valleys and ranges. (c) Geologic map of the southern half of the Grant Range (modified from Long & Walker, 2015). Abbreviations: SCT = Schofield Canyon thrust; TMA = Timber Mountain anticline.

accommodated by a system of brittle normal faults that were active at low (<20°) dip angles, which has exhumed granite and greenschist-facies metasedimentary rocks from depths up to ~10 km (e.g., Fryxell, 1988; Long & Walker, 2015; Lund et al., 1993). Published geochronology indicates that extension on this low-angle fault system was underway by ~29 Ma (Long & Walker, 2015); however, the duration of extension is not constrained. In this study, we integrate multipart cooling histories of granite samples exhumed in the footwall of the low-angle fault system in the southern Grant Range with a sequentially

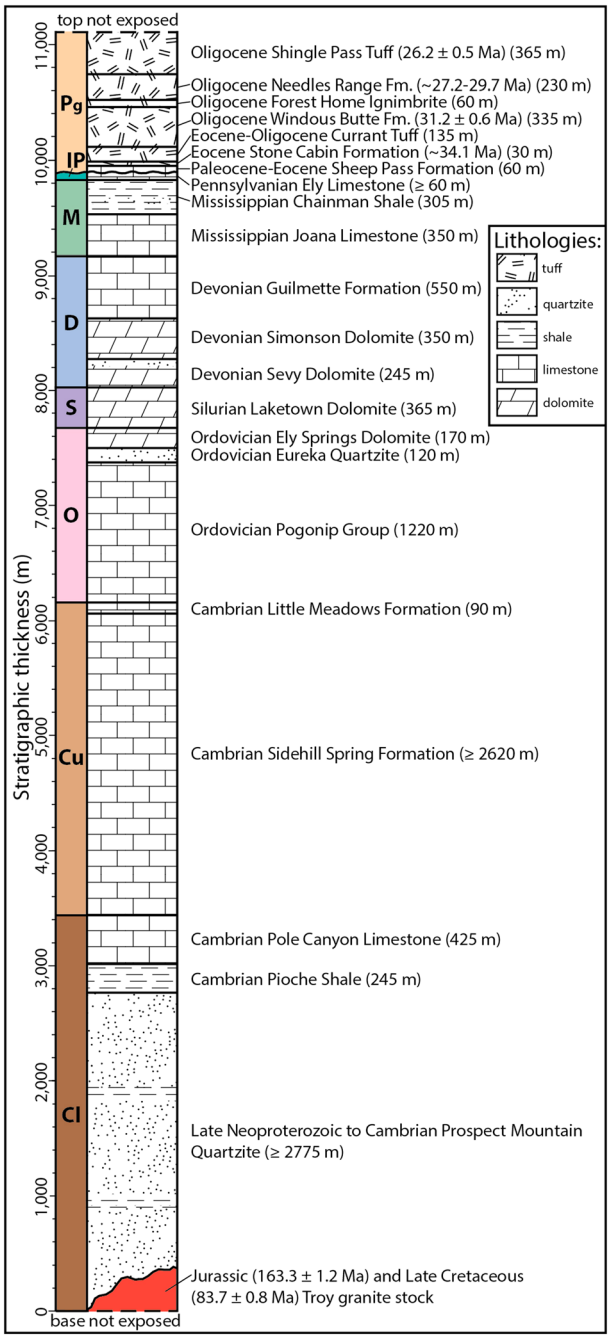

Figure 2. Stratigraphic column for the southern Grant Range. The colored portion of the column shows the grouped stratigraphic divisions used on Figure 3. Ages shown for the Needles Range and Stone Cabin Formations are K-Ar biotite ages from Kleinhampl and Ziony (1985), and ages shown for the Shingle Pass Tuff and Windous Butte Formation are $^{40}Ar/^{39}Ar$ sanidine ages from Taylor et al. (1989).

restored cross section, in order to constrain the timing and rates of extension accommodated by this unique fault system. We then explore the implications of this timing record for the spatiotemporal evolution of extensional tectonism in eastern Nevada and western Utah, and speculate on the geodynamic processes that controlled the transition of the Cordillera from a contractional to an extensional regime. In addition, this project also serves as a case study that demonstrates the utility of muscovite $^{40}Ar/^{39}Ar$ multi-diffusion domain modeling as an effective technique for constraining the cooling histories of rocks between ~425 and ~250 °C.

2. Tectonic Setting

During the late Neoproterozoic and Paleozoic, eastern Nevada was a site of dominantly shallow-marine sedimentation (e.g., Stewart, 1980). During the Jurassic to Paleogene (~150–50 Ma) construction of the Cordilleran orogenic belt, eastern Nevada occupied part of the broad hinterland of the Sevier fold-thrust belt (e.g., Armstrong, 1972; DeCelles, 2004; Yonkee & Weil, 2015). During Cordilleran orogenesis, crustal shortening in eastern Nevada was accommodated by thrust faults and folds at upper-crustal levels (e.g., Bartley & Gleason, 1990; Long, 2012, 2015; Long et al., 2014; Taylor et al., 2000) and by ductile thickening at middle- and lower-crustal levels (e.g., Cooper et al., 2010; Hallett & Spear, 2014; Lewis et al., 1999; McGrew et al., 2000). By the terminal stages of thickening in the latest Cretaceous-Paleocene, a high-elevation plateau (the "Nevadaplano") is interpreted to have existed in eastern Nevada, which attained crustal thicknesses up to ~50–60 km (Figure 1a; Allmendinger, 1992; Chapman et al., 2015; Coney & Harms, 1984; DeCelles & Coogan, 2006).

During and after Cordilleran orogenesis, eastern Nevada underwent a protracted transition to an extensional setting. Spatially isolated Late Cretaceous to Paleocene (~80–60 Ma) extension, which was contemporaneous with the final stages of shortening in the Sevier thrust belt, has been documented (e.g., Camilleri & Chamberlain, 1997; Druschke, Hanson, Wells, Rasbury, et al., 2009; Hodges & Walker, 1992; Long et al., 2015), and has been interpreted to have been initiated by lithospheric delamination (Wells & Hoisch, 2008). Eocene-Oligocene extension has also been documented (e.g., Gans & Miller, 1983; Gans et al., 1989, 2001; Druschke, Hanson, & Wells, 2009; Evans et al., 2015; Lee et al., 2017; Long & Walker, 2015), and was often associated spatially and temporally with the Great Basin ignimbrite flare-up, a NE to SW sweep of silicic volcanism interpreted to have accompanied post-Laramide slab rollback (Figure 1a; e.g., Dickinson, 2002; Humphreys, 1995). The initiation of widespread extension that formed the Basin and Range Province, which is attributed to establishment of the San Andreas transform system (e.g., Atwater, 1970), was not until the middle Miocene (e.g., Cassel et al., 2014; Colgan & Henry, 2009; Dickinson, 2002).

3. Grant Range Stratigraphy, Magmatism, Metamorphism, and Brittle Detachment System

The Grant Range contains a 10-km-thick section of Cambrian to Pennsylvanian sedimentary rocks, which are dominated by carbonates (Figure 2; e.g., Camilleri, 2013; Fryxell, 1988; Moores et al., 1968). In the southern Grant Range, Cambrian rocks have been folded into an E-vergent, recumbent anticline (the Timber

10.1029/2018TC005073

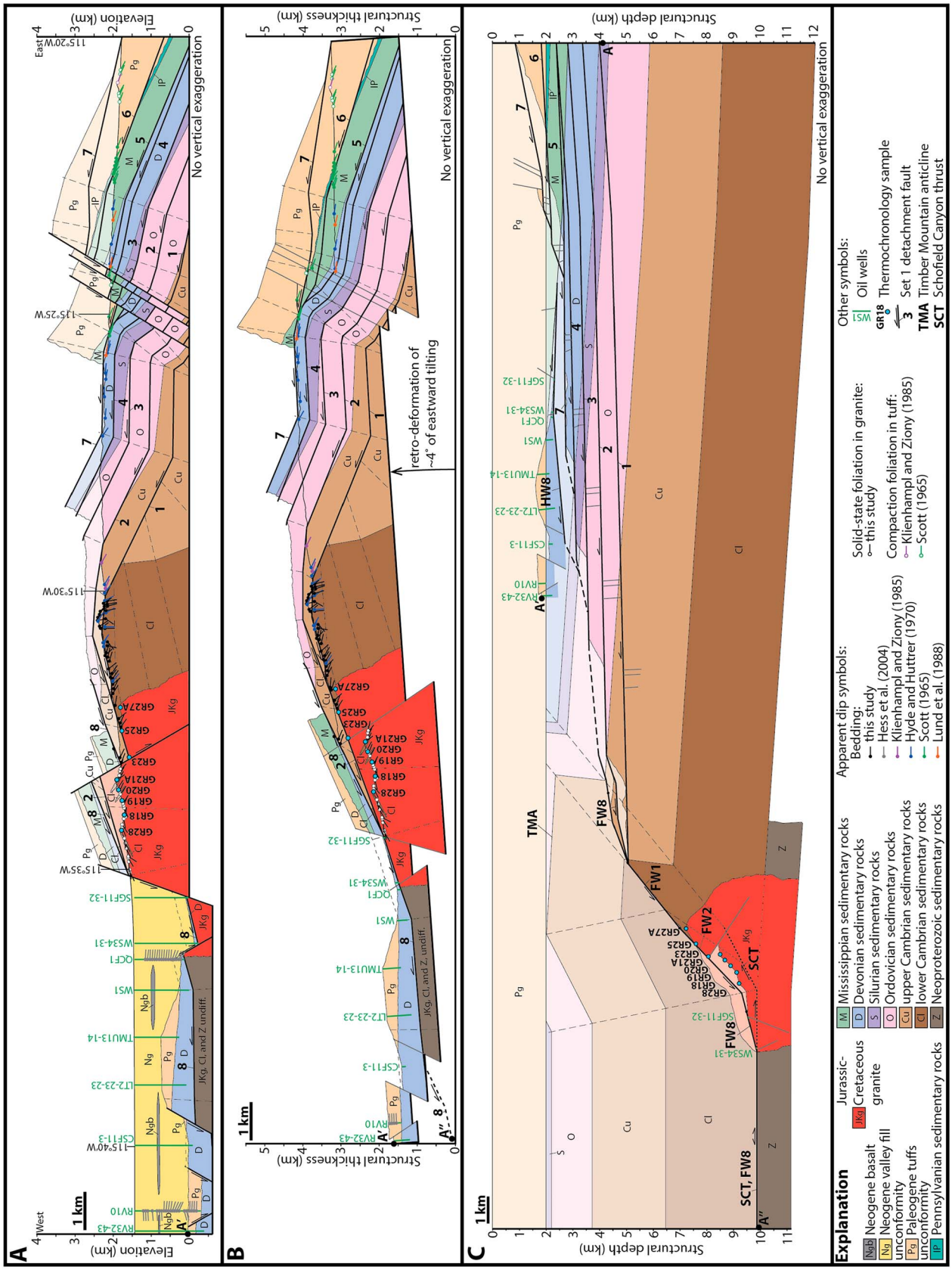

Figure 3. (a) Cross section A-A′, showing the present-day geometry. The translucent areas above the modern erosion surface represent eroded rock. Oil well locations are shown on Figure S2. (b) Cross section A-A′ after retro-deformation of set 2 faults (see the supporting information for methods). (c) Cross section A-A′ after retro-deformation of offset on set 1 faults (note: shown at a different scale than (a) and (b)). The Paleogene unconformity is restored to horizontal. A 2.0-km thickness of Paleogene rocks is shown, after thicknesses observed in other parts of the southern Grant Range (Moores et al., 1968; Scott, 1965; Taylor et al., 1989), and minimum thicknesses reported in the Pancake Range to the west (Ekren et al., 1972). For Faults 1, 2, and 8, the restored positions of rocks in their footwall (FW) and hanging wall (HW) are shown. After set 1 extension, point A′ in the hanging wall of Fault 8 was placed above point A" in its footwall; these are the reference points used to estimate cumulative set 1 extension.

Mountain anticline of Fryxell, 1988) and are intruded by the Troy granite stock (Figures 1 and 2), which has Jurassic and Late Cretaceous components (Lund et al., 2014; Taylor et al., 2000). On the western margin of the stock, a boudinaged granite sill, which predates folding, yielded a U–Pb zircon crystallization age of 163.3 ± 1.2 Ma, and undeformed granite that makes up the majority of the stock, and postdates folding, yielded an 83.7 ± 0.8 Ma crystallization age (Lund et al., 2014). Cambrian sedimentary rocks experienced greenschist-facies metamorphism during the Late Cretaceous intrusion event (Camilleri, 2013; Fryxell, 1988; Long & Soignard, 2016).

Paleozoic sedimentary rocks are unconformably overlain by Paleogene rocks, including the Paleocene-Eocene Sheep Pass Formation, and late Eocene to Oligocene rhyolitic ash-flow tuffs deposited during the Great Basin ignimbrite flare-up. Six tuffs are exposed in the southern Grant Range, and range in age between ~34.1 and ~26.2 Ma (Figure 2; Kleinhampl & Ziony, 1985; Scott, 1965; Taylor et al., 1989). A minimum thickness of 1.25 km of Paleogene rocks is exposed on the studied transect, but in other parts of the southern Grant Range the Paleogene section is as thick as 1.7–2.1 km (Lund et al., 1993; Moores et al., 1968; Scott, 1965; Taylor et al., 1989). On the studied transect, Paleogene rocks overlie Mississippian-Pennsylvanian rocks in the eastern part of the range (Figures 1 and 3; Long, 2014; Lund et al., 1988, 1993; Scott, 1965), and overlie Devonian rocks within oil wells in Railroad Valley (Figure 3; Hess et al., 2004).

The Grant Range is deformed by a system of west-vergent, brittle detachment faults (used here to denote normal faults that dip less than 30°), which characteristically exhibit low (<15°) cutoff angles with stratigraphy (Figures 1 and 3; Camilleri, 2013; Long & Walker, 2015; Lund et al., 1993). After Long and Walker (2015), we refer to these as set 1 faults. In the central Grant Range, 4–6 km north of the studied transect, Long and Walker (2015) documented that the set 1 fault system grew from bottom to top into an imbricate stack, through progressive excision. Isostatic rebound accompanying tectonic thinning resulted in syn-extensional folding of the set 1 system across an anticlinal culmination, as indicated by progressively increasing interlimb angles observed on younger, structurally higher faults (Long & Walker, 2015). The final geometry consists of an imbricate stack of ~5–25° E-dipping, back-rotated faults in the eastern part of the range, and a series of ~5–30° W-dipping faults in the western part (Lund et al., 1993). Retro-deformation of folding indicates that set 1 faults were active at ~5–15° dip angles (Long & Walker, 2015).

The duration of set 1 faulting is not precisely constrained, but field relations help bracket motion timing. On the eastern side of the range, tuffs as young as ~32 Ma are cut by set 1 faults (Long, 2014; Lund et al., 1987, 1988, 1993; Scott, 1965). In the western part of the central Grant Range, a ~29 Ma dacite dike cuts the structurally lowest (and oldest) set 1 faults (Camilleri, 2013; Long & Walker, 2015). K-Ar white mica ages of 25.3 ± 0.5 Ma and 23.1 ± 0.5 Ma (originally reported in Armstrong, 1970 but recalculated by Taylor et al., 1989) from the Troy granite stock have been interpreted to date cooling triggered by tectonic denudation during set 1 faulting (Bartley et al., 1984; Fryxell, 1984; Taylor et al., 1989).

After set 1 faulting, extension of likely Miocene to Quaternary age was accommodated along high-angle normal faults, including structures that accommodated the subsidence of Railroad Valley (Figures 1 and 3; Camilleri, 2013; Fryxell, 1988; Lund et al., 1993). After Long and Walker (2015), we refer to these high-angle faults as set 2 faults. In the northern Grant Range, the ~16–9 Ma Horse Camp Formation was deposited during set 2 faulting (Horton & Schmitt, 1998; Moores et al., 1968), and is time-equivalent to the basal sedimentary fill in Railroad Valley (Horton & Schmitt, 1998; Johnson, 1993). Subhorizontal Pliocene basalt flows are intercepted in oil wells in Railroad Valley, near the top of the valley fill section (Figure 3; Hulen et al., 1994), which indicates minimal Pliocene to recent tilting. The down-to-west normal fault system that bounds the western side of the Grant Range exhibits Quaternary scarps (Camilleri, 2013; Long, 2014).

4. Structural Model for Extension in the Southern Grant Range

4.1. Deformed Cross Section, and Restoration of Set 2 Extension

Geologic mapping from this study (see Figure S1 in the supporting information) and from published studies was compiled to support drafting cross section A-A′ across the southern Grant Range (Figure 3a). Map data from Scott (1965), Kleinhampl and Ziony (1985), and Lund et al. (1988) were compiled in the eastern half of the range, and map data from Hyde and Huttrer (1970), Fryxell (1988), and this study were compiled in the western half. Lithologic logs of nine oil wells in Railroad Valley were projected onto the cross section

Table 1
Summary of Crosscutting Relationships and Geometric and Offset Constraints for Set 1 Detachment Faults on Cross Section A-A′

Fault number	Dip angle at modern erosion surface or constrained by well data	Cutoff angle with stratigraphy at modern erosion surface or constrained by well data	Fault offset (m)	Stratigraphic omission range (m)	Crosscutting relationships
8	22°W (between trace and well SGF11-32)	3° (hanging wall, western Grant Range)	4,300	3350–6100 m (east of intersection with fault 1)	cuts Fault 2 (required)
	14°W (between wells SGF11-32 and WS34-31)	48–69° (footwall; above eastern flank of TMA)		8600–9200 m (west of intersection with fault 1)	
7	12°E minimum (west of western trace)	4° (between two traces)	900	200–250 m (east of intersection with faults 5–6)	cuts or merges with Fault 6 (required)
	16°E (between two traces)	4° maximum (footwall; west of trace)		900–1200 m (west of intersection with faults 5–6)	cuts ~27.2–29.7 Ma volcanics (observed)
6	12°E minimum (east of trace)	5° maximum (assuming constant cutoff angles across-strike)	1,750	100–200 m	cuts or merges with Fault 5 (required)
	20°E (based on cutoff angle constraint)				cuts ~31.2 Ma volcanics (required)
5	10–15°E minimum (in the shallow subsurface)	4° maximum (east of intersection with Fault 6)	3,500	100–250 m	
4	10°E minimum (west of trace)	5° maximum (assuming constant cutoff angles across-strike)	3,000	250 m	merges with Fault 3 (observed)
	25°E (based on cutoff angle constraint)				
3	5°E minimum (west of trace)	5° (interpreted)	3,050	250 m	cuts Fault 2 (observed)
2	10°E minimum (at eastern trace)	20–64° (above eastern flank of TMA)	3,700	350 m	cuts Fault 1 (observed)
	17°W (at western trace)				
1	5°E (between easternmost two traces)	42–57° (hanging wall; above eastern flank of TMA)	3,350	350 m (east of TMA)	
	10°W (between middle traces)	29–46° (footwall; above upright limb of TMA)		1950–3150 m (within TMA)	
	12°W (between westernmost two traces)	100–118° (footwall; above overturned limb of TMA)			

Note. Observations that support folding of Faults 1 and 2 are highlighted in gray. TMA is the Timber Mountain anticline.

(see the supporting information for supporting data), and logs of apparent dip magnitude were available from two wells (Hess et al., 2004).

Apparent dips of bedding were projected onto A-A′ and were used to delineate dip domains separated by kink surfaces (e.g., Suppe, 1983). The dip angles of set 1 faults were estimated using geometric constraints on the cross section and three-point problems (see the supporting information for supporting data) and were integrated with the dip domains to calculate cutoff angles with stratigraphy (Table 1). Angular relationships and contacts offset across faults were drafted so that they are retro-deformable. Therefore, the cross section represents a viable solution (Elliott, 1983). Figure 3b shows a version of A-A′ with tilting and motion accommodated by set 2 faults restored (details on methods in the supporting information). Four degrees of eastward tilting was estimated for A-A′, which is corroborated by gentle (typically $\leq$5°) apparent dips within Neogene valley fill sediment in two oil wells. Comparison of the pre-set 2 length (29.0 km) and post-set 2 length (31.4 km) yields 2.4 km of extension (8%).

4.2. Geometry and Kinematics of Set 1 Extension

On A-A′, the set 1 fault system consists of eight distinct detachment faults (detailed descriptions of each fault are included in the supporting information), which all omit stratigraphic section, cut down-section toward the west, and consistently offset matching stratigraphic cutoffs westward. Most set 1 faults exhibit m-scale breccia zones (Fryxell, 1988; Long & Walker, 2015; Lund et al., 1993), and several exhibit gouge (Fryxell, 1988), indicating brittle conditions during extension (we acknowledge that this does not preclude the possibility of ductile deformation early during the motion history of some of the older, structurally deeper faults;

however, no ductile fault zone rocks were definitively identified in the field). Crosscutting relationships (summarized on Table 1) demonstrate that structurally lower faults are cut by structurally higher faults, indicating bottom-up development, similar to observations in the central Grant Range (Long & Walker, 2015).

The eastern half of the range contains a vertically stacked series of ~5–20° E-dipping, ~300- to 600-m-thick sheets carried by Faults 1–7, which exhibit typical cutoff angles of ~5°. Toward the west, Faults 5 and 6 either merge with, or are cut by, Fault 7 in the subsurface, and Faults 3, 4, and 7 project westward above the modern surface. Faults 1–5 have individual offset magnitudes that range between 3.0 and 3.7 km, and Faults 6 and 7 exhibit 1.7 km and 0.9 km of offset, respectively. Fault 6 cuts rocks as young as the ~31.2 Ma Windous Butte Formation, and Fault 7 cuts rocks as young as the ~27.2–29.7 Ma Needles Range Formation. The Paleogene unconformity overlies Pennsylvanian rocks on the eastern margin of the range, and overlies Mississippian rocks further to the west. This observation, combined with similar dip magnitudes below and above, defines minimal (≤4°) angularity across the Paleogene unconformity.

In the western half of the range, Faults 1 and 2 are folded across the axial zone of a broad anticlinal culmination. East of the culmination axis, Faults 1 and 2 dip ~15–20°E, and west of the axis they dip ~15–20°W, defining an interlimb angle of ~140–150°. After the structural model of Long and Walker (2015), construction of the culmination is interpreted as the result of isostatic rebound that accompanied progressive tectonic denudation during set 1 extension. Within the axial zone of the culmination, Faults 1 and 2 deform Cambrian rocks that lie within the Timber Mountain anticline, an E-vergent, recumbent fold with a steeply dipping to overturned lower limb and an upright upper limb (Fryxell, 1988; Figures 1 and 3). As a result, cutoff angles on these faults increase westward. Cutoff angles on Faults 1 and 2 are as high as ~60–120° where they deform portions of the lower limb, and are between ~30–45° where they carry rocks that restore within the upright limb.

On the western flank of the range, Fault 8 places Devonian rocks over Cambrian rocks, and cuts Fault 2 (Figure 3). Here Fault 8 exhibits a hanging wall cutoff angle of ~3°, and footwall cutoff angles in Cambrian rocks that restore within the lower limb of the Timber Mountain anticline are as high as ~70°. Fault 8 is correlated with a fault intercepted in the easternmost two wells in Railroad Valley (SGF11-32 and WS34-31), which places Devonian rocks over granite (Figure 3). Fault 8 exhibits as much as ~8–9 km of stratigraphic omission, which is by far the largest omission of any set 1 fault on the cross section (Table 1). Therefore, after Long and Walker (2015), we interpret that Fault 8 represents a master detachment level, into which the cumulative offset from all structurally lower set 1 faults to the east was fed. Rocks that can be matched up across the footwall and hanging wall of Fault 8 are not present on the area of the cross section, and therefore only the minimum structural overlap (11.7 km) can be estimated. It is difficult to discern how much of this overlap is the result of motion on Fault 8, versus motion cumulatively added from the structurally lower set 1 faults to the east. However, the Devonian stratigraphic level of the Paleogene unconformity in wells in Railroad Valley, combined with the east-west extent of Devonian rocks preserved in the hanging wall of Fault 8, constrains the restored position of these rocks (Figures 3b and 3c), and indicates that an additional 4.3 km of offset on Fault 8 is necessary to place point A′ over point A".

The Paleogene unconformity is intersected in four wells in Railroad Valley, which are spread across an E-W distance of 6 km (Figure 3). In all four wells, the Devonian Guilmette Formation underlies Paleogene rocks. This relationship implies minimal angular discordance across the unconformity, limiting it to a maximum of ~5°. Between the eastern part of the range and Railroad Valley, the Paleogene unconformity cuts gently down section toward the west, from the base of the Pennsylvanian section to the top of the Devonian section (Figure 3c). This indicates a total Paleogene structural relief of ~1.0 km for rocks that restore to the east of the Timber Mountain anticline.

4.3. Retro-Deformation of Set 1 Extension

Restoration of offset on set 1 faults was performed by matching the locations of offset stratigraphic cutoffs (Figure 3c). Because minimum thicknesses were utilized for several stratigraphic units (see the supporting information for details), and because drafting decisions sought to minimize fault offset where possible, the cumulative extension estimate should be considered a minimum.

Due to the polyphase extension accommodated in the Grant Range, determination of pre-set 1 dip magnitudes of Paleozoic rocks in all areas of the cross section is difficult. Multiple across-strike exposures of the

Paleogene unconformity, which define minimal angularity (≤4–5°) and a maximum of ~1.0 km of pre-extensional structural relief, aided retro-deformation of Paleozoic rocks that restore to the east of the Timber Mountain anticline. However, as the Timber Mountain anticline is complexly dismembered by set 1 faults, and much of the western portion of the fold has been obscured by granite that postdates folding, reconstructing its geometry is difficult. Its present-day geometry indicates that it is an E-vergent anticline, with a vertical to overturned forelimb and an upright backlimb (Fryxell, 1988). We interpret that the most likely structural mechanism to produce this geometry is fault-propagation folding above an E-vergent thrust fault (e.g., Suppe & Medwedeff, 1990).

Between 5 and 20 km along-strike to the south, three E-vergent thrust faults that deform Cambrian-Devonian rocks have been mapped (Bartley & Gleason, 1990; Fryxell, 1988; Taylor et al., 2000). These thrust faults are correlated with the Central Nevada thrust belt, a system of E-vergent, Mesozoic contractional structures interpreted as a hinterland component of the Sevier thrust belt (e.g., Taylor et al., 2000). However, northward continuations of these thrust faults have not been mapped at the latitude of the cross section, or further to the north in the Grant Range (Long & Walker, 2015; Moores et al., 1968). The Schofield Canyon thrust can be traced as close as ~6 km south of the cross section line (Figure 1), where it places Cambrian rocks over Ordovician rocks (Fryxell, 1988, 1991). Fryxell (1988) interpreted that growth of the Timber Mountain anticline is related to motion on this thrust fault. We expand on this interpretation, and model the Timber Mountain anticline as a fault-propagation fold that grew above the Schofield Canyon thrust (Figure 3c). Twelve km along-strike to the south of the section line, rocks as deep as the Ordovician Pogonip Group underlie the Paleogene unconformity (Bartley & Gleason, 1990; Long, 2015). Therefore, we drafted the Timber Mountain anticline so that the Paleogene unconformity lies within Ordovician rocks over its crest zone (Figure 3c). This corresponds to a structural height of ~2.0 km for the anticline. On the western end of the cross section, the Schofield Canyon thrust is shown with a flat at the base of the Cambrian section, which ramps up section to the east. This geometry is interpretive, and is based on observation of a 3.4-km-thick section of lower Cambrian rocks in the footwall of Fault 1 that is undisturbed by faults. Therefore, the geometry shown represents the highest permissible regional level for the Schofield Canyon thrust. The lower Cambrian rocks are likely underlain by at least 3–4 km of Neoproterozoic sedimentary rocks, based on sections documented further to the east, north, and south in Nevada (e.g., Stewart, 1980). The root zone of the Timber Mountain anticline has been overprinted by the Troy stock, which postdates folding. On Figure 3c, the Schofield Canyon thrust and Timber Mountain anticline are constructed with dashed lines through the stock. These relationships are schematic, and are meant to illustrate a simple interpretation of the original geometry of the fold.

On Figure 3c, the set 1 fault system (specifically, the fault plane that contains preserved portions of the footwalls of Faults 1, 2, and 8) is shown steepening to a dip of ~40°W where it intersects the crest and backlimb of the Timber Mountain anticline. This is a consequence of the observed cutoff angles on the faults, the stratigraphic levels that they occupy, and the interpreted pre-extensional geometry of the anticline. This geometry produces a ~5 km tall, W-dipping ramp in the set 1 fault system. At the base of the ramp, Fault 8 is interpreted to sole westward into a flat at the base of the Cambrian section that was originally activated as the E-vergent Schofield thrust. This geometry is speculative, as rocks buried to these levels are not exposed at the surface. However, the following points justify this geometric interpretation as viable: 1) the backlimb of the Timber Mountain anticline provided mechanically favorable bedding orientations for the formation of moderately W-dipping, bedding-subparallel normal faults; 2) a stratigraphic horizon that was originally activated as the Schofield Canyon thrust would be an ideal pre-existing weakness for the set 1 fault system to sole into and reactivate; and 3) an analogous extensional system in eastern Nevada, the Northern Snake Range decollement, also rooted into a bedding-subparallel horizon within the lower Cambrian section (Gans et al., 1985; Miller et al., 1983).

To estimate cumulative set 1 extension, pre-extensional and postextensional lengths on Figure 3c were compared. Point A is defined in the footwall of Fault 1 on the eastern edge of the cross section. Point A′ is defined at the western extent of the hanging wall of Fault 8. The restored (pre-set 1 extension) E-W distance between points A and A′ is 20.7 km. Point A" is defined in the footwall of Fault 8 at the western edge of the cross section. Over the duration of set 1 extension, Point A′ was translated westward and placed above point A". The E-W distance between points A and A" is 44.3 km. Therefore, the minimum cumulative extension accommodated by the set 1 fault system is 23.6 km (114%).

Table 2
Cooling Ages for the Irwin Canyon Granite Samples

Sample	Latitude (dd. ddddd)	Longitude (dd. ddddd)	Elevation (m)	Pre-set 1 depth (km)	Sample context	MAr (Ma; ±1σ)	ZFT (Ma; ±1σ)	ZHe (Ma; ±2σ)	AFT (Ma; ±1σ)	AHe (Ma; ±2σ)
GR27A	38.36908	115.53506	2,090	7.3	foliated granite; no country rock present in outcrop	65.4 ± 0.3	24.8 ± 1.3	17.51 ± 0.38	17.1 ± 2.1	13.41 ± 0.68
GR25	38.37394	115.54294	1,975	7.6	foliated granite; no country rock present in outcrop	56.7 ± 0.2	24.6 ± 1.7	11.83 ± 0.22	18.8 ± 2.9	18.32 ± 0.88
GR23	38.37917	115.55019	1,880	8.1	foliated granite; no country rock present in outcrop	59.9 ± 0.3	29.2 ± 1.9	10.96 ± 0.20	18.9 ± 2.2	19.92 ± 0.49
GR21A	38.38375	115.55714	1,795	8.5	foliated granite; no country rock present in outcrop	42.7 ± 0.3	24.0 ± 1.1	13.28 ± 0.24	17.6 ± 2.4	20.66 ± 0.75
GR20	38.38664	115.55942	1,760	8.7	foliated granite; no country rock present in outcrop	28.0 ± 0.2	22.7 ± 2.6	10.19 ± 0.25	18.7 ± 2.4	15.22 ± 0.42
GR19	38.38953	115.56264	1,725	8.9	deformed, m-scale sill intruding Cambrian limestone	28.7 ± 0.3	23.9 ± 1.3	12.27 ± 0.29	17.1 ± 1.8	-
GR18	38.39217	115.56692	1,680	9.2	boudinaged 1 m-thick sill intruding Cambrian quartzite	28.3 ± 0.2	23.4 ± 1.6	11.19 ± 0.20	17.6 ± 2.1	18.23 ± 0.35
GR28	38.39611	115.57167	1,635	9.3	deformed 30 cm-thick sill intruding Cambrian quartzite	25.5 ± 0.2	21.7 ± 1.2	12.07 ± 0.20	16.2 ± 1.7	12.57 ± 0.40

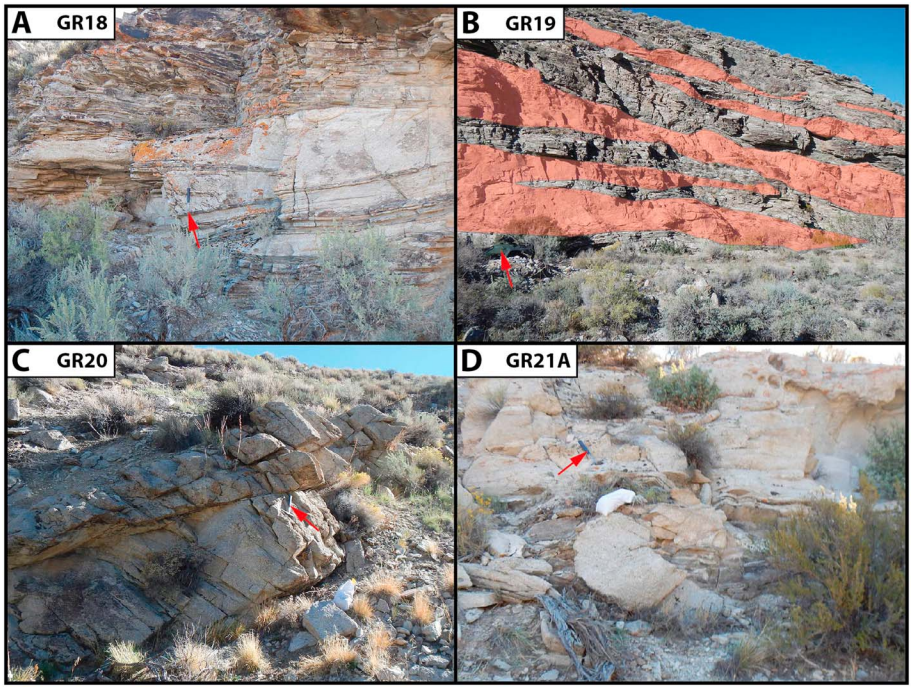

Figure 4. Photographs showing field relations of granite samples. (a) Outcrop where sample GR18 was collected, from a ~1-m-thick, deformed granite sill of likely Jurassic age intruded into the Cambrian Prospect Mountain Quartzite. Red arrow points to rock hammer, and is the site of sampling. (b) Multiple meter-scale, boudinaged granite sills (highlighted in red) intruded into the Cambrian Pole Canyon limestone. Sample GR19 was collected from the lowest sill. View is facing SW. Red arrow points to all-terrain vehicle for scale. (c and d) Outcrops where samples GR20 and GR21A were collected. Both were collected from massive granite outcrops within the main body of the Troy pluton, which are likely of Late Cretaceous age. Red arrows point to a rock hammer, and also demarcate the sites of sampling.

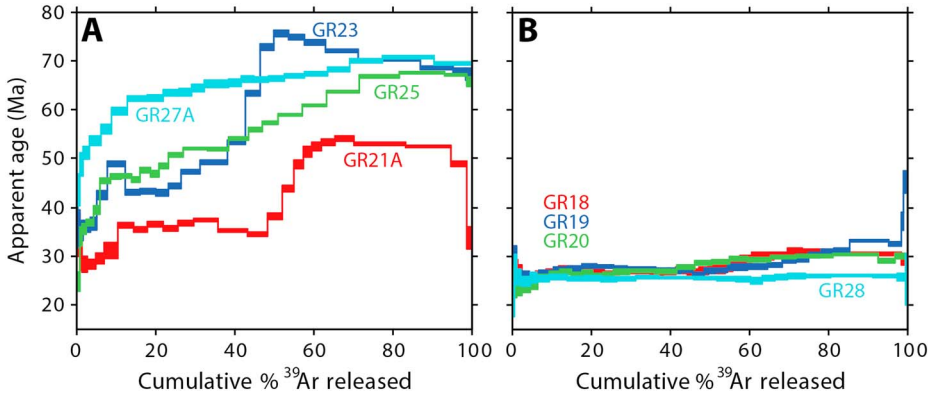

Figure 5. $^{40}Ar/^{39}Ar$ age spectra plots for the Irwin Canyon granite samples. A shows spectra for the shallowest, easternmost four samples, and B shows spectra for the deepest, westernmost four samples.

5. Set 1 Extension Timing From Thermochronology Integrated With Sequential Restoration

5.1. Cooling Ages and Rates of Irwin Canyon Granite Samples

Eight granite samples were collected from the Troy stock, along Irwin Canyon in the western part of the range (Figure 1c and Table 2). The three westernmost samples (GR28, GR18, and GR19) were collected from deformed sills intruded into lower Cambrian rocks in the western flank of the range (Figures 4a and 4b). These sills were likely emplaced during the Jurassic (~163 Ma), based on dating of a similar boudinaged granite sill by Lund et al. (2014). The five easternmost samples (GR20, GR21A, GR23, GR25, and GR27A) were collected from the main body of weakly deformed to undeformed, Late Cretaceous (~84 Ma; Lund et al., 2014) granite that comprises the bulk of the Troy stock (Figures 4c and 4d). On the restored cross section (Figure 3c), these samples span structural depths of 7.3–9.3 km below the top of the Paleogene section, which is interpreted as the approximate surface level. The restored depths of the samples decrease toward the east. All samples lie in the footwall of Fault 2, west of its intersection with Fault 1, and therefore are autochthonous relative to the set 1 fault system. In order to quantify the timing and rates of denudation-induced cooling during set 1 faulting, we collected composite cooling histories from muscovite, zircon, and apatite separated from all eight granite samples.

Muscovite $^{40}Ar/^{39}Ar$ (MAr) ages were collected at the New Mexico Geochronology Research Laboratory (see the supporting information for supporting data and details on methodology). The age spectra exhibit variably developed age gradients that correlate to structural depth. For instance, the shallowest, easternmost

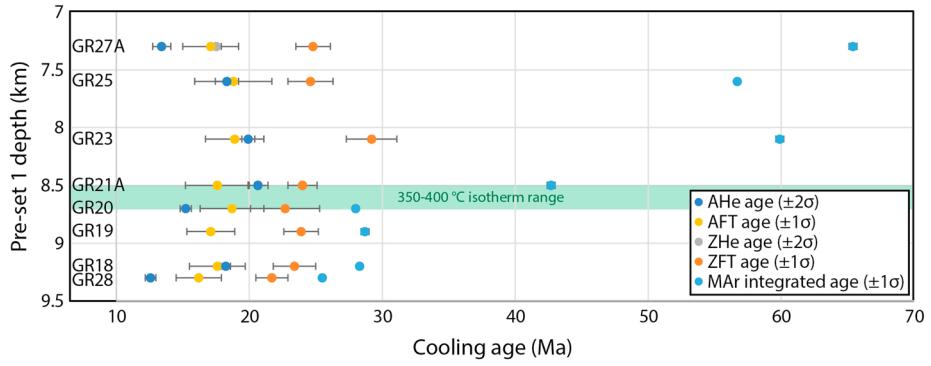

Figure 6. Cooling ages plotted versus pre-set 1 depth. Integrated MAr ages are plotted, and only the ZHe age from sample GR27A is plotted (the younger, inverted ZHe ages are not shown; see discussion in the text). An inflection point at ~28 Ma is defined for the integrated MAr ages between depths of ~8.5 km (sample GR21A) and ~8.7 km (sample GR20). This represents the depth range below which samples were above the MAr bulk closure temperature of ~350–400 °C at ~28 Ma. This defines a ~40–47 °C/km geothermal gradient range at ~28 Ma. This graph also demonstrates that all eight samples were fully reset for the ZFT, AFT, and AHe thermochronometric systems.

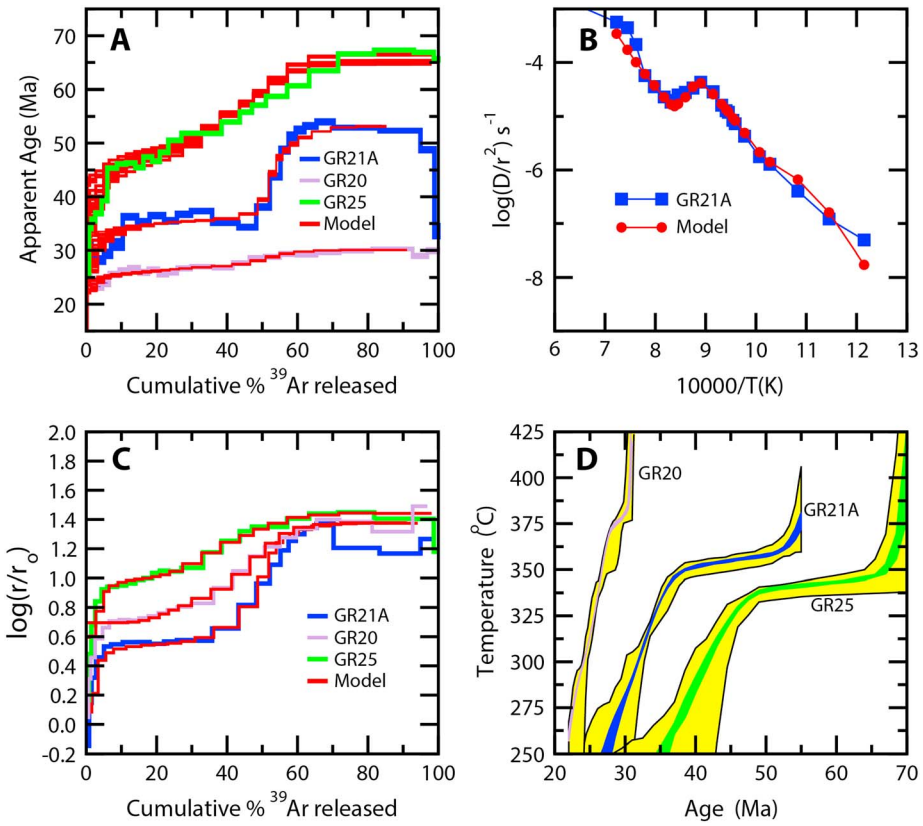

Figure 7. $^{40}Ar/^{39}Ar$ muscovite MDD model examples. (a) Model and measured age spectra for samples GR21A, GR20, and GR25. Spectra have the characteristic form of MDD behavior, showing intermediate flat segments and inflections indicative of variable diffusion length scales; (b) Arrhenius plot for measured and modeled data for GR21A. All Arrhenius plots for muscovite samples in this study are similar and exhibit a characteristic "knee" consistent with MDD behavior; (c) $\log(r/r_o)$ plots utilizing an E of 63 kcal/mol and a $\log(D_0/r_o^2)$ value that begins the spectrum at zero by convention. The shape of the $\log(r/r_o)$ plots are highly correlated to the shape of the age spectra, which again is consistent with MDD behavior; (d) cooling histories derived from the MDD method. Each model requires temperatures greater than 350–400 °C prior to the oldest part of each age spectrum with variable cooling histories corresponding to variable paleodepths.

four samples (GR27A, GR25, GR23, and GR21A) yielded integrated ages between 42.7 ± 0.3 and 65.4 ± 0.3 Ma, and their spectra record age gradients that begin near ~25–30 Ma and climb to ~50–70 Ma (Figures 5a and 6). In contrast, the deepest, westernmost four samples (GR20, GR19, GR18, and GR28) yielded integrated ages between 25.5 ± 0.2 and 28.7 ± 0.3 Ma and have much less pronounced age gradients ranging between ~25 and ~30 Ma (Figures 5a and 6). Taken as a group, the MAr integrated ages define a pattern that suggests that passage through the bulk closure temperature for muscovite (~350–400 °C) occurred later in the more deeply buried rocks compared to the more shallowly buried rocks.

However, rather than linking the muscovite integrated ages to a bulk closure temperature, we propose that the age spectra and ^{39}Ar release data are amenable to thermal history investigation by multi-diffusion domain (MDD) modeling. Here we expand on the methodology for extracting continuous thermal histories from muscovite based on a MDD model. The MDD method for K-feldspar (Lovera et al., 1989) is well established and in many cases can provide geologically consistent thermal histories with important implications for tectonic interpretations. Because MDD is a volume diffusion based model it requires transport of argon in nature and in the laboratory via diffusion, and since K-feldspar is anhydrous there is a reasonable expectation that this phase remains stable during argon extraction. Mineral stability during in vacuo argon extraction for a hydrous mineral such as muscovite may be a less reasonable expectation; however, there is evidence that diffusion can occur in muscovite under laboratory conditions. For instance, like shown here, there are numerous examples in the literature that document age gradients in muscovite spectra that suggest that the spatial distribution of argon can be recovered via step heating (e.g., Baldwin & Harrison, 1989;

Dallmeyer & Villeneuve, 1987; Heizler et al., 1997; West & Lux, 1993). Also, although not well documented in the literature, there is often a relationship between laboratory temperature and muscovite grain size, where finer-grained muscovite separates release more gas at lower temperature compared to coarser-grained muscovite separates (e.g., Heizler, 1994). This is a requirement of the MDD model if grain size represents the effective diffusion length scale. In addition to these observations, Harrison et al. (2009) demonstrated that a MDD approach for laboratory degassed muscovite may provide a means to recover thermal histories. They documented a grain size relationship for $^{40}Ar^*$ loss that conformed to a diffusion model, but only briefly discussed using ^{39}Ar to recover grain size distributions. Heizler and Harrison (2009) expanded on this data set and showed that MDD modeling of the ^{39}Ar produced kinetic parameters that, when forward modeled with the known preirradiation thermal history, predicted the measured age spectrum for each of the experimental diffusion runs. Harrison and Lovera (2013) followed with a muscovite example that showed the potential to invert a natural dataset to achieve a continuous thermal history between ~400 and 300 °C. Forster and Lister (2014) also argued that the release of ^{39}Ar in vacuo could be used to deconvolve kinetic parameters for mixtures of muscovite and phengite, again suggesting that the MDD approach can be applied to white mica $^{40}Ar/^{39}Ar$ data.

In this study, we measured muscovite via the furnace step-heating method and found that most samples yielded well-defined age gradients (Figure 5). The spectra conform to a pattern indicative of a nonuniform grain size distribution (i.e., inflections and intermediate flat sections) that prompted us to explore the possibility of utilizing the MDD approach to obtain thermal histories. In Figure 7, we use samples GR20, GR21A, and GR25 to illustrate the muscovite MDD approach (supporting data for all samples are shown in the supporting information). The Arrhenius data are determined from the fraction of ^{39}Ar released and the temperature and duration of each heating step (Figure 7b). For clarity, only the Arrhenius data for GR21A are shown on Figure 7b, and they display the characteristic "knee" reflecting the exhaustion of gas from small domains transitioning to the degassing of larger domains. Harrison et al. (2009) determined an activation energy (E) of 63 ± 7 kcal/mol for the muscovite Arrhenius law and that value is used here for construction of the $\log(r/r_o)$ plots shown in Figure 7c. The slope of the initial diffusion coefficients on the Arrhenius plot is less than 63 kcal/mol and is presumably caused by simultaneous degassing of multiple small diffusion domains (cf. Lovera et al., 1993). However, the high-temperature slope segments match well with the E determined by Harrison et al. (2009), as shown by the intermediate flat segments on the $\log(r/r_o)$ plots. The $\log(r/r_o)$ plots are highly characteristic of MDD behavior and are well correlated with their corresponding individual age spectra. That is, inflections on the $\log(r/r_o)$ spectra are positioned similarly to positions on the age spectra, which for samples with protracted cooling is again a hallmark of the MDD model.

Model data are shown in red in Figures 7a–7c. The Arrhenius and thus $\log(r/r_o)$ data are well described by the MDD model, with only minor misfit for sample GR21A for the highest temperature steps. Using the kinetic data models, thermal histories (Figure 7d) were determined by forward-modeling the measured age spectra (e.g., Lovera et al., 1989). All samples are required to be above ~400 °C prior to the oldest part of each age spectrum, with GR25 and GR21A showing relatively long residence near 350 °C from the late Cretaceous into the Eocene, with cooling through ~250 °C by about 40 and 30 Ma, respectively. Consistent with its overall flat age spectrum, sample GR20 cooled from ~400 °C at ~30 Ma and passed below 300 °C by 25 Ma. We note that this closure temperature range is defined by the release of ^{39}Ar under laboratory conditions, where the extraction furnace is held at essentially 0 kbar. This is in contrast to the closure temperatures reported by Harrison et al. (2009) for $^{40}Ar^*$ loss at 10 and 5 kbar. Harrison et al. (2009) reported closure temperatures of 420 °C and 405 °C for 10 and 5 kbar, respectively for a cooling rate of 10 °C/Myr and an effective diffusion radius of 100 μm. Samples here underwent $^{40}Ar^*$ loss at approximately 2–2.5 kbar (see depth estimates above) and thus using ^{39}Ar at 0 kbar underestimates the geologic closure temperature of the Grant Range samples by ~10–15 °C. This is a small offset considering a host of other uncertainties of the models (i.e., true E), and also the MDD models do not have a single 100 μm diffusion length scale as assumed by Harrison et al. (2009) in their example closure temperature calculation. We cannot quantitatively estimate the actual diffusion length scales without accurate knowledge of D_o, but since the samples are variably deformed there is every expectation that individual mica grains represent fragments with variable effective diffusion radii.

The MDD modeling provides information on the timing and rates of cooling from ~425 to ~250 °C for seven of the Irwin Canyon granite samples. The four deepest samples exhibit similar temperature-time (T-t) paths

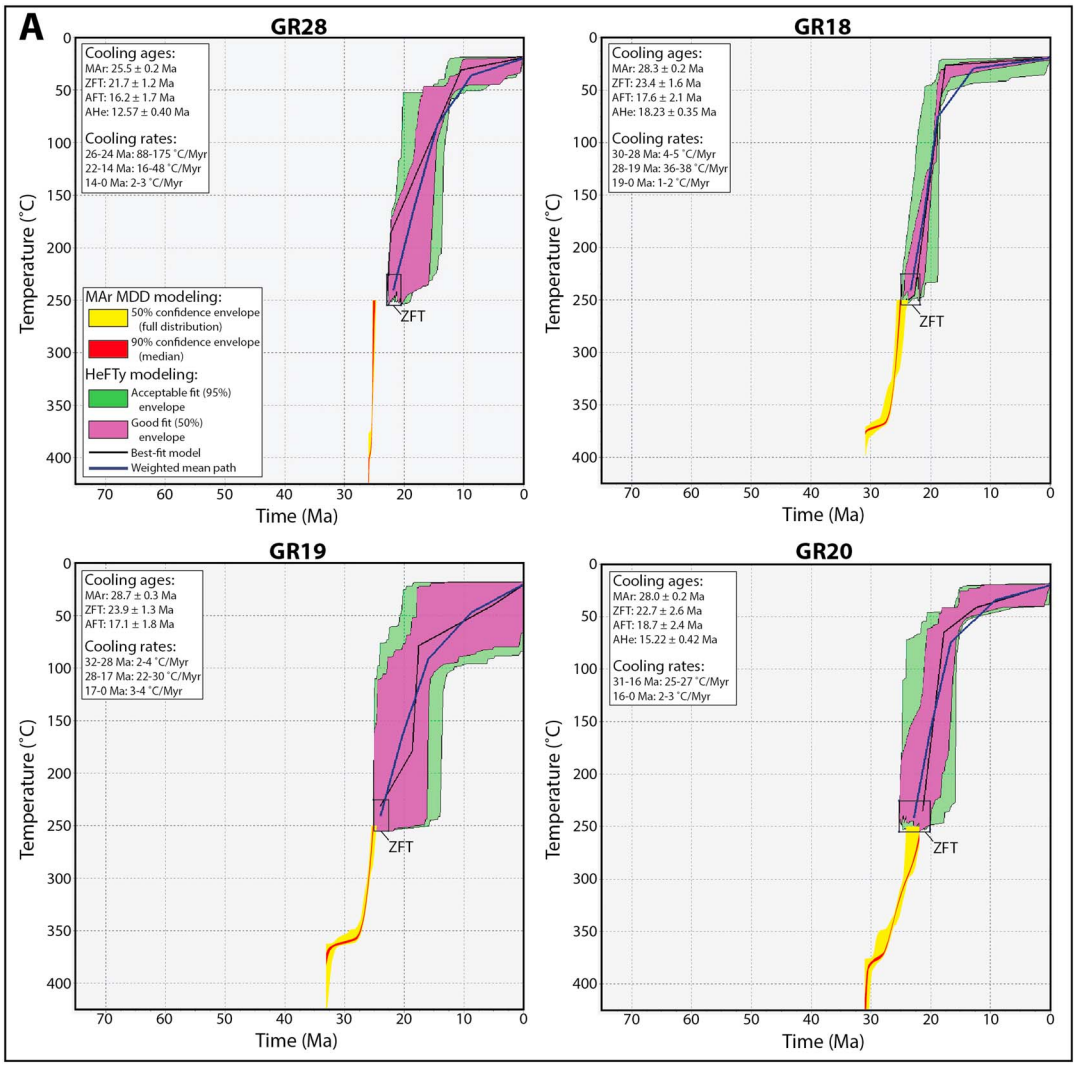

Figure 8. Composite T-t paths for the granite samples ((a) and (b) show paths for the deepest and shallowest four samples, respectively), which combine the ~425 to ~250 °C paths obtained from MAr MDD modeling (yellow envelope is the 90% confidence interval of the MDD-derived cooling histories, and red envelope is the 90% confidence interval of the median, after Quidelleur et al., 1997) with the ~250 to ~20 °C paths obtained from HeFTy modeling of ZFT, ZHe, AFT, and AHe ages (green and pink envelopes, and associated best-fit and weighted mean paths). ZFT data were entered as a constraint in T-t space with a closure temperature range of 240 ± ~15 °C (Bernet, 2009); see the supporting information for details.

(Figure 8a), with GR18, GR19, and GR20 cooling rapidly from 375–425 to 250 °C between 28–31 and 22–25 Ma, at typical rates of ~20–35 °C/Myr, and GR28 exhibiting exceptionally rapid cooling from 425 to 250 °C between 26 and 24 Ma. MDD T-t paths were obtained from three of the four shallowest samples, which exhibit slow to moderate cooling (typical ~1–10 °C/Myr range) that spans between ~70 and ~25 Ma (Figure 8b). Sample GR21A cooled from 375 to 350 °C between 55 and 37 Ma (1 °C/Myr), and from 350 to 250 °C between 37 and 26 Ma (9 °C/Myr). Sample GR25 cooled from 400 to 350 °C between 70 and 67 Ma (17 °C/Myr), from 350 to 335 °C between 67 and 48 Ma (1 °C/Myr), and from 335 to 250 °C from 48 to 34 Ma (6 °C/Myr). Sample GR27A cooled from 370 to 250 °C between 71 and 46 Ma (5 °C/Myr).

Zircon (ZFT) and apatite fission track (AFT) ages were collected at the University of Arizona Fission Track Laboratory (supporting data and methods in the supporting information). ZFT and AFT ages are interpreted to record cooling through closure temperatures of ~240 °C (for a cooling rate of 15 °C/Myr; Bernet, 2009) and ~120 °C (for apatite of average composition at a cooling rate of 10 °C/Myr; Reiners & Brandon, 2006), respectively. ZFT ages range between 21.7 ± 1.7 and 24.8 ± 1.3 Ma, with one outlying age of 29.2 ± 1.9 Ma (GR23;

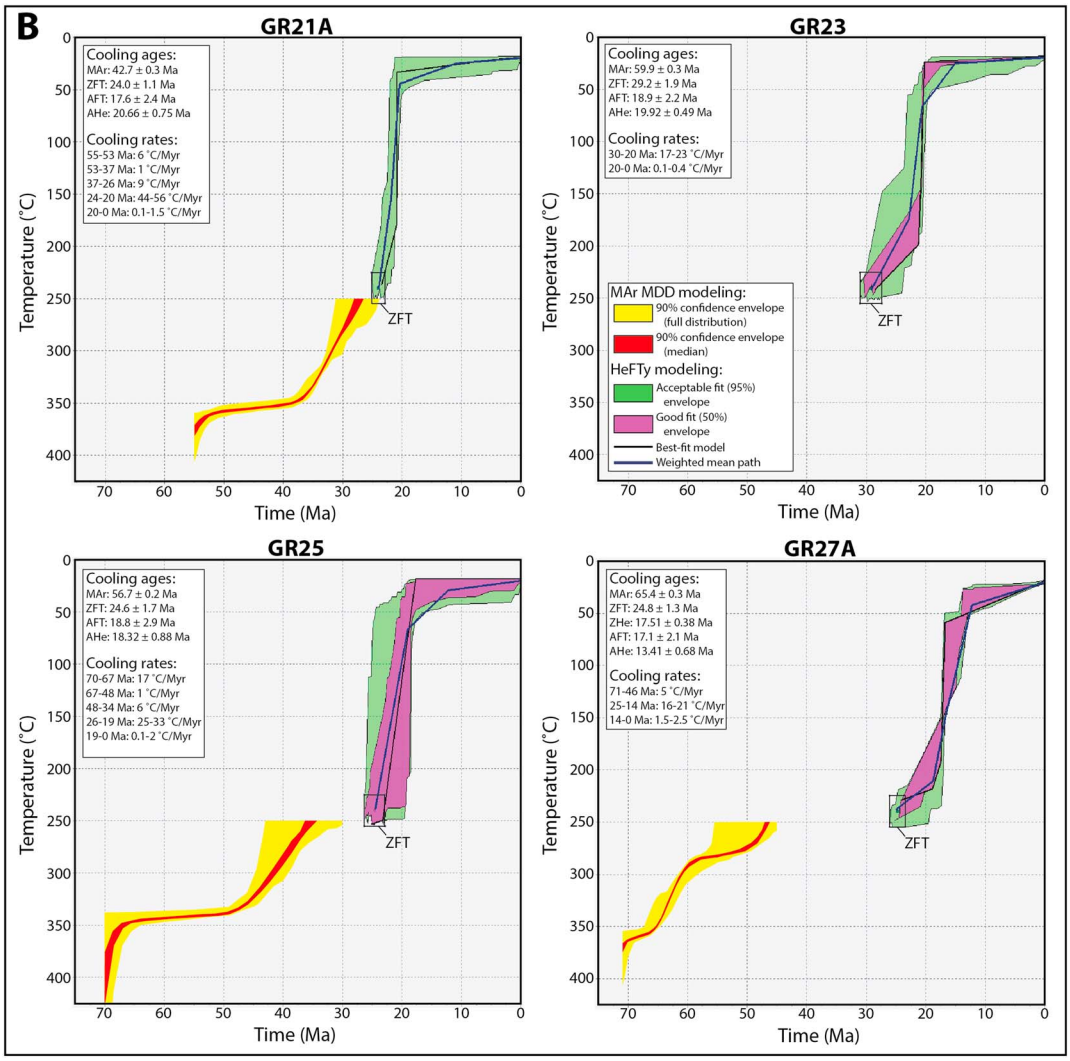

Figure 8. (continued)

Figure 6; Table 2). AFT ages all overlap within error, with a total range between 16.2 ± 1.7 and 18.9 ± 2.2 Ma (Figure 6; Table 2). These ages are similar to AFT ages of 15.6 ± 0.4 and 14.8 ± 1.7 Ma obtained from the Troy granite stock by Stockli (1999).

(U-Th)/He ages were collected from apatite (AHe) and zircon (ZHe) at the University of Arizona Radiogenic Helium Dating Laboratory (see supporting information for supporting data and methods). At a cooling rate of ~10 °C/Myr, ZHe and AHe ages are interpreted to date cooling through closure temperatures of ~180 ± 10 °C (Reiners et al., 2004) and ~65 ± 5 °C (Flowers et al., 2009), respectively. The AHe ages range between 12.57 ± 0.40 and 20.66 ± 0.75 Ma (Figure 6; Table 2). AHe ages from four of the samples (GR18, GR21A, GR23, and GR25) overlap within error with the AFT ages from the corresponding samples.

Sample GR27A yielded a ZHe age of 17.51 ± 0.38 Ma, which overlaps with the AFT age from this sample, and is ~4 Myr older than the corresponding AHe age. However, the ZHe ages from the other seven samples range between 10.96 ± 0.25 and 13.28 ± 0.24 Ma, and are typically between 4 and 8 Myr younger than the AFT and AHe ages from the corresponding samples (Table 2). This inversion in cooling ages is interpreted as the result of extreme zonation within the analyzed zircons that resulted in U-enriched rims and tips, which led to anomalously high alpha ejection (e.g., Hourigan et al., 2005; Orme et al., 2015). This interpretation is supported by photomicrographs of the zircon grains and mica external detectors that were utilized to collect the ZFT ages from these samples, which exhibit a high concentration of natural and induced fission tracks in the rims, by a

positive age-eU correlation that is consistent with U zonation, and by low Th/U values that are consistent with overgrowth of Th-poor metamorphic rims (e.g., Orme et al., 2015; supporting graphs, photomicrographs, and text are included in the supporting information). In light of this zonation, and the consistency within and between the AFT and AHe datasets, the inverted ZHe ages for these seven samples are not interpreted to be representative of the timing of exhumation-related cooling, and were not incorporated into the thermal modeling.

The ZFT, AFT, and AHe ages (and the ZHe age from sample GR27A) were inverse-modeled using the program HeFTy (Ketcham, 2005) to quantify T-t paths from ~250 °C to surface temperatures (see the supporting information for methods and modeling parameters; Figure 8). The HeFTy T-t paths from all eight samples illustrate a similar pattern of rapid cooling (typical rates of ~20–35 °C/Myr) from 225–255 to 25–50 °C, followed by slower cooling (typical rates of ~1–3 °C/Myr) to surface temperatures. The transition from rapid to slow cooling has a total range between ~14 and ~20 Ma, but on average is 17 ± 2 Ma (1σ).

Combining the T-t paths obtained from HeFTy and MAr MDD modeling from the five deepest samples (GR28, GR18, GR19, GR20, and GR21A) defines one episode of rapid cooling (at typical rates of 20–35 °C/Myr) from 350–425 to 25–50 °C between 28–31 Ma (with an outlying value of 37 Ma) and 15–19 Ma. The MDD models from the two shallowest samples record a more protracted T-t history, with GR25 cooling from 425 to 250 °C between 70 and 34 Ma, and GR27A cooling from 375 to 250 °C between 71 and 46 Ma. However, the HeFTy models from these two samples, as well as from sample GR23 where MAr MDD data were not available, show cooling histories similar to the deepest five samples for the ≤250 °C portion of the T-t path. The apparent disagreement between the MAr MDD and HeFTy paths for samples GR25 and GR27A is partly due to the sensitivity of the MDD models in the ~250 °C temperature range, and the fact that the MDD and HeFTy models were run independent of each other. For instance, the youngest age in the muscovite age spectrum for GR25 is 24 Ma, but only represents 0.8% of the total ^{39}Ar released. This indicates that the smallest diffusion domain was open to argon loss at this time, which is compatible with the HeFTy model for this sample. However, the automated MDD thermal modeling doesn't do a good job of fitting this tiny gas fraction, but rather focuses on the larger and older gas fraction. Manually forcing the thermal history for the muscovite through the ZFT age at ~240 °C would not significantly impact the goodness of fit for the muscovite model age spectrum, and thus is completely compatible for the muscovite data. A similar argument can be made for GR27A. The initial age gradient in the muscovite spectrum is very steep and could project to younger ages than actually measured and modeled, and keeping the sample at or above 240 °C until ~25 Ma (the ZFT age) would have very little impact on the goodness of fit of the MAr MDD model. The MAr MDD model is not very sensitive to the thermal history trajectory between 250 and 225 °C, and thus the apparent mismatch between the MDD and HeFTy paths for these samples is mostly related to projecting at constant cooling rate from 45 to 25 Ma rather than slowing the cooling, as suggested by the discordance in age between the youngest argon ages and the ZFT age. Formally incorporating the full muscovite MDD model into the HeFTy code would avoid this projection and can perhaps be utilized in future efforts to invert muscovite MDD data when lower temperature constraints are available.

5.2. Set 1 Extension Timing From Integration of Cooling and Depth Histories

Figure 9 shows six forward-modeled increments of cross section A-A′ (performed using Midland Valley Move; see the supporting information for methods and input parameters), which illustrates the geometric evolution of the set 1 fault system and allows tracking the depths of the granite thermochronology samples. Over the duration of set 1 extension, the granite samples were exhumed from an initial depth range of 7.3–9.3 km to depths ranging between 1.1 and 1.6 km (Figure 10). Therefore, set 1 extension is predicted to have resulted in significant exhumation-related cooling. Thus, we interpret that the episode of rapid (20–35 °C/Myr) cooling from 350–425 to 25–50 °C between 28–31 and 15–19 Ma dates the duration of motion on the set 1 fault system. This timing range is consistent with several dated field relationships from the Grant Range and surrounding areas, including (1) A ~29 Ma dacite dike that cuts the oldest set 1 faults in the central Grant Range (~5 km north of the studied transect), indicating that extension had begun by the late Oligocene (Long & Walker, 2015); (2) 20 km to the south in the Quinn Canyon Range, an early episode of normal faulting took place between ~32 and ~27 Ma, as bracketed by ^{40}Ar/^{39}Ar ages of pre-extensional and postextensional igneous rocks (Taylor et al., 1989); (3) On the studied transect, Fault 7 cuts a ~27.2–29.7 Ma tuff, which defines a maximum motion age. Similarly, ~5–15 km to the north, tuffs as young as ~32 Ma are cut by set 1 faults

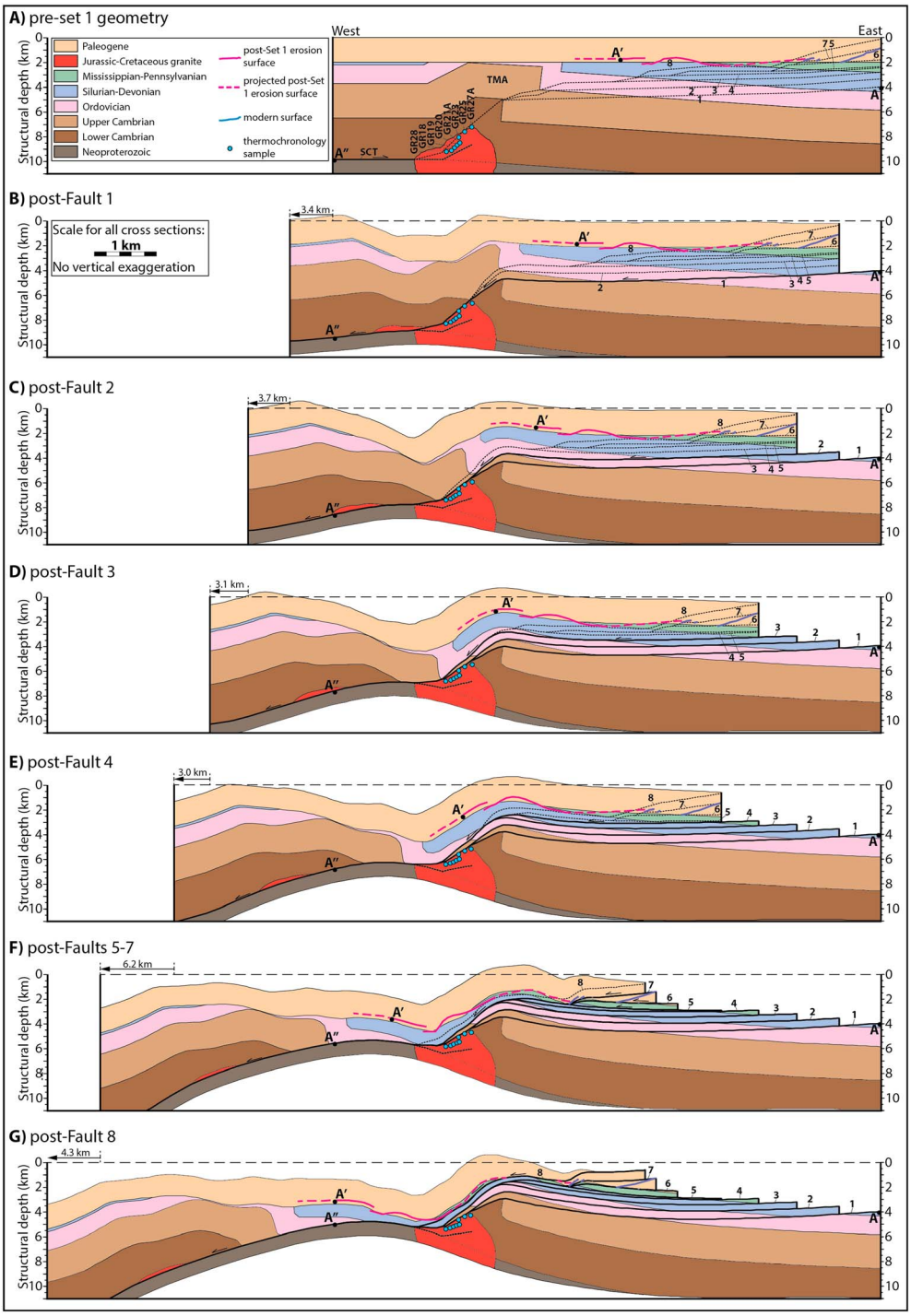

Figure 9. Sequentially deformed increments of cross section A-A′, showing the evolution of the deformation geometry over the duration of set 1 extension. Sequential forward modeling of deformation and isostatic decompaction were performed using Midland Valley Move 2017.2 (see the supporting information for methods and modeling parameters). Extension magnitudes during each increment are based on offset magnitudes of individual set 1 faults (Figure 3 and Table 1). Markers that allow for more precise estimation of the depth of the granite thermochronology samples during the later stages of set 1 extension include the observed level of the post-set 1 erosion surface, as supported by well data in Railroad Valley, and proximal projections of the post-set 1 erosion surface to the east and west (to the east, the lowest level of the post-set 1 erosion surface is constrained by the modern erosion surface exposed in the hanging walls of Faults 6 and 7). Abbreviations: SCT = Schofield Canyon thrust; TMA = Timber Mountain anticline.

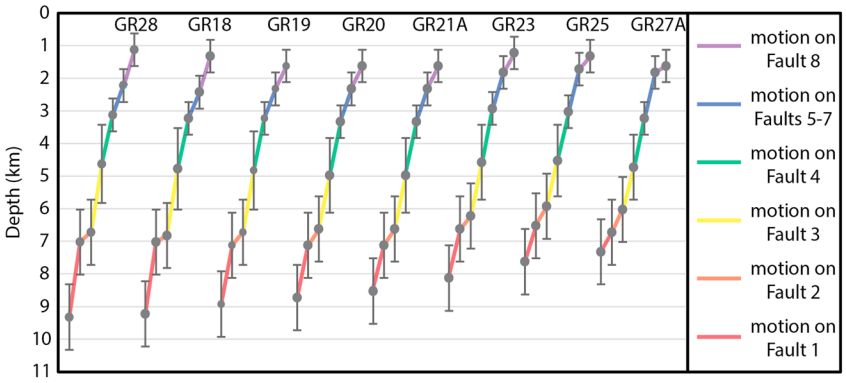

Figure 10. Graph tracking depths of the granite samples over the duration of set 1 extension. Depths were measured on Figure 9. Initial depths and depths after motion on Faults 1 and 2 were measured relative to the top of the Paleogene section, and were assigned approximate error values of ±1 km. Errors for depths after motion on Fault 3 were assigned by the difference between the top of the Paleogene section and the projected post-set 1 erosion surface. Depths after motion on Faults 4, 5–7, and 8 were measured relative to the post-set 1 erosion surface, and were assigned approximate error values of ±0.5 km.

(Long & Walker, 2015; Lund et al., 1988, 1993); and (4) K-Ar white mica ages of ~25.3 and ~23.1 Ma from the Troy stock have been interpreted to date cooling during set 1 faulting (Bartley et al., 1984; Fryxell, 1984; Taylor et al., 1989).

The 23.6 km of cumulative set 1 extension is bracketed over a duration of 9–16 Myr, which defines a long-term extension rate of 1.5–2.6 km/Myr. This is faster than the typical ~0.5–1.0 km/Myr displacement rates documented on individual Basin and Range normal faults (e.g., Nicol et al., 1997). However, this rate is not unusual for metamorphic core complexes, which have documented extension rates that can range up to 7–9 km/Myr or higher (e.g., Davis & Lister, 1988; Foster et al., 1993; Ketcham, 1996; Rey et al., 2009; Spencer & Reynolds, 1991; Wells et al., 2000).

The transition from rapid (20–35 °C/Myr) to slow (1–3 °C/Myr) cooling that occurred at 15–19 Ma is interpreted to bracket the maximum permissible age for the initiation of set 2 extension, which exhumed the granite samples from temperatures of ~25–50 °C and depths of 1.1–1.6 km to the modern surface. Set 2 faults that were likely responsible for much of this exhumation include a down-to-east fault that lies between samples GR23 and GR21A (Figure 3a), and the down-to-west, range-bounding fault system that borders the eastern side of Railroad Valley (Figures 1 and 3). Initial subsidence within Railroad Valley is interpreted to be dated by deposition of late Miocene valley fill sediments (Effimoff & Pinezich, 1981; Horton & Schmitt, 1998; Hulen et al., 1994; Johnson, 1993).

Combining the initial ~350–425 °C temperatures and 8.5–9.3 km depths of the five westernmost granite samples indicates an approximate geothermal gradient range of ~40–45 °C/km at the initiation of set 1 extension (~31–28 Ma). This is similar to the ~40–47 °C/km geothermal gradient range at ~28 Ma defined by the inflection point in MAr integrated ages on Figure 6. The late Oligocene (~32–28 Ma) was the approximate timing of initial felsic magmatism associated with the Great Basin ignimbrite flare-up in this part of Nevada (e.g., Henry & John, 2013), and therefore, addition of magmatic heat may have been responsible for elevated geothermal gradients at this time. Also, there are several small (tens of meters thick or less, $\leq$ ~0.5 km map length) Oligocene granite and dacite dikes mapped in the Grant Range (Figure 1c), two of which have been dated at ~31.7 Ma (Lund et al., 2014) and ~29 Ma (Long & Walker, 2015). Therefore, though restored sample depth is interpreted as the primary control on the variations observed in the integrated MAr ages and MDD T-t histories (Figures 5, 6, and 8), it is also possible that local variations in heating due to proximity to Oligocene dikes could explain some of these variations, in particular between the adjacent samples GR20 and GR21A.

Long and Soignard (2016) used multiple thermometers to estimate a ~60 °C/km peak upper-crustal thermal field gradient in the central Grant Range, which was attained during the ~84 Ma intrusion of the Troy stock, and produced the greenschist-facies metamorphism observed in Cambrian and Ordovician sedimentary rocks (Camilleri, 2013; Fryxell, 1988; Lund et al., 1993). The protracted cooling histories recorded by the

MAr MDD data from the shallowest two granite samples (GR25 and GR27A), which extend as far back as ~70 Ma, are interpreted to record a combination of the relaxation of this Late Cretaceous peak thermal regime and any erosion that predated set 1 extension and ignimbrite flare-up volcanism. These shallower samples were evidently not sufficiently re-heated prior to set 1 extension to reset their MAr MDD T-t histories.

Figure 9 illustrates the possibility for development of a syn-extensional basin in the hanging wall of the set 1 fault system, which may have locally generated as much as ~2 km of accommodation space. The most likely location of any potential syn-extensional sediments would be under Railroad Valley. As most wells in Railroad Valley do not present any age control for valley fill sediments (Hess et al., 2004), it is possible that the basal portion of the valley fill section locally contains late Oligocene to early Miocene sediments. However, a more likely scenario is that much of the accommodation space generated during set 1 extension was filled with a nearly continuous supply of regionally sourced late Oligocene to early Miocene tuffs. Anomalously thick sections of ~30–22 Ma tuffs in the Grant Range and adjacent parts of the Pancake Range to the west (Ekren et al., 1972; Scott, 1965), as well as field relations between tuffs in the Grant Range (Scott, 1965), may provide support for this.

The two youngest tuffs in the Grant Range, the 28.5 ± 1.3 Ma Needles Range Formation (Taylor et al., 1989) and ~27.2–29.7 Ma Shingle Pass Tuff (Kleinhampl & Ziony, 1985), temporally overlap with the early stages of set 1 extension. Two kilometers south of the studied transect, these tuffs have a total thickness of ~0.8 km (Scott, 1965). Scott (1965) documented ~0.4 km of cumulative thinning of these tuffs toward the northwest of the section line, and up to ~3° of angularity across their contacts, over a map distance of ~5 miles. Over this same distance, ~0.2 km of the underlying Windous Butte Formation is truncated and is overlain by the Needles Range Formation across an angular unconformity (Scott, 1965). It is possible that these field relationships are the result of syn-extensional deformation during basin infilling. However, as tuffs can change thickness over relatively short distances, often as a result of paleotopography (e.g., Henry et al., 2011), these field relationships are equivocal.

In proximal areas of the Pancake Range, tuffs and lavas deposited between ~30.3 and ~22.1 Ma, which overlap with the first ~6–9 Myr of set 1 extension, exhibit minimum thicknesses of ~1.3–1.9 km (Dixon et al., 1972; Ekren et al., 1972; Ekren, Hinrichs, et al., 1973; Ekren, Rogers, & Dixon, 1973; Kleinhampl & Ziony, 1985; Snyder et al., 1972). With a consistent source of air fall and outflow material from proximal calderas to the west (Henry & John, 2013), it is possible that infilling of any accommodation space generated by set 1 extension was dominated by volcanics.

6. Discussion

Extension in Nevada and Utah is interpreted to have accommodated the collapse of the Cordilleran orogenic plateau (e.g., Allmendinger, 1992; Colgan & Henry, 2009; Coney & Harms, 1984; DeCelles, 2004). Therefore, analysis of the timing and distribution of extension has the potential to elucidate the geodynamic processes that govern orogenic collapse. However, the transition of the Cordilleran plateau to an extensional regime was complex in space and time, and several aspects of this evolution remain enigmatic (e.g., Dickinson, 2002; Colgan & Henry, 2009; Druschke, Hanson, & Wells, 2009; Henry et al., 2011; Long, 2012; Wells et al., 2012). In particular, the magnitudes, spatial patterns, and driving mechanisms of extension that predates the middle Miocene reorganization of the Pacific-North American plate boundary to a transform system, and the corresponding inception of widespread extension that constructed the Basin and Range Province (e.g., Colgan & Henry, 2009; Dickinson, 2002, 2006; Faulds & Henry, 2008), remain subjects of ongoing debate (e.g., Axen et al., 1993; Best et al., 2009; Druschke, Hanson, & Wells, 2009; Gans et al., 1989; Henry et al., 2011). The Grant Range detachment system provides an important piece of this puzzle, as the results of this study demonstrate that it was one of the most significant fault systems to accommodate extension prior to the middle Miocene. Here the Grant Range fault system is placed in the larger framework of Eocene-Oligocene extension within the Cordilleran orogenic plateau, in order to speculate on the geodynamic processes that contributed to the transition to an extensional regime during the final stages of subduction. This discussion is supported by a compilation of documented sites of Paleogene and older extension across central and eastern Nevada and western Utah (Table 3 and Figure 11).

By the end of shortening in the Sevier thrust belt in the Paleocene (e.g., DeCelles, 2004; Yonkee & Weil, 2015), the crust in eastern Nevada had attained a peak thickness of ~50–60 km (Figure 11; e.g., Chapman et al., 2015;

Table 3
Compilation of Published Late Eocene-Oligocene (and Older) Extension Timing Estimates From Eastern and Central Nevada and Western Utah

Number on Figure 11	Location	Data source	Extension timing	Timing relative to volcanism	Explanation of supporting data
1	Little Clear Creek half graben	Constenius (1996)	38–31 Ma	overlaps	Syn-extensional tuffaceous rocks and sediments deposited in half graben in Sevier fold thrust belt
2	Santaquin Meadows half graben	Constenius (1996)	38–33 Ma	overlaps	Syn-extensional tuffaceous rocks and sediments deposited in half graben in Sevier fold thrust belt
3	Juab Valley	Constenius (1996)	39–27 Ma	overlaps	Syn-extensional tuffaceous rocks and sediments deposited in half graben in Sevier fold thrust belt
4	Sevier Valley	Constenius (1996)	39–27 Ma	overlaps	Syn-extensional tuffaceous rocks and sediments deposited in half graben in Sevier fold thrust belt
5	Sanpete Valley	Constenius (1996)	39–27 Ma	overlaps	Syn-extensional tuffaceous rocks and sediments deposited in half graben in Sevier fold thrust belt
6	Northern Mineral Mountains	Coleman and Walker (1990)	>25 Ma	uncertain	25 Ma granodiorite cuts normal faults in northern Mineral Mountains
7	Beaver Lake Range	Lemmon and Morris (1984); Axen et al. (1993)	>25 Ma	uncertain	Normal faults overlapped by granodiorite correlated with 25 Ma granodiorite in northern Mineral Mountains
8	Wah Wah Mountains	Friedrich and Bartley (1992)	>32–33 Ma	uncertain	Normal faults overlapped by basal Oligocene (~32–33 Ma) volcanic rocks
9	The Needles	Axen et al. (1993)	>34–32 Ma	uncertain	Normal faults overlapped by 34–32 Ma Escalante Desert Formation
10	Deep Creek Range	Gans et al. (1991)	37–34 Ma	overlaps	Early (37–34 Ma) pulse of rapid cooling defined by 40Ar/39Ar and fission-track thermochronometry
11	Eastern Kern Mountains	Gans et al. (1989); Miller et al. (1999)	35–24 Ma	syn	Earliest extension above NSRD was coeval with Kalamazoo volcanics at 35 Ma; early episode of extension over by 24 Ma
12	Northernmost Snake Range	Gans et al. (1989)	39–35 Ma	syn	Dacite intrusion overlaps normal faults in hanging wall of NSRD, and is also offset by NSRD; tuffs overlap normal faults
13	Northern Snake Range	Lee et al. (2017)	37.8–22.5 Ma	overlaps	U–Pb zircon dating of deformed and undeformed rhyolite dikes brackets timing of fabric development
14	Northern Snake Range	Lee and Sutter (1991)	37–24 Ma	overlaps	40Ar/39Ar cooling histories from muscovite, biotite, and K-feldspar interpreted to date timing of mylontic deformation
15	Northern Snake Range	Lee (1995)	48–41 and 30–26 Ma	pre, overlaps	Rapid cooling pulses observed in K-feldspar 40Ar/39Ar multi-diffusion domain modeling interpreted as denudation timing
16	Northern Snake Range	Gébelin et al. (2014)	49–45 and 27–21 Ma	pre, overlaps	Eocene muscovite 40Ar/39Ar ages on western flank of range, Miocene ages on eastern flank
17	Southern Snake Range	Miller et al. (1999)	32–15 Ma	overlaps	Total range of apatite fission track ages is ~32–20 Ma in western part of range and ~19–15 Ma in eastern part
18	Southern Snake Range	Evans et al. (2015)	50–38, 33–23, and 23–8 Ma	pre, overlaps	Modeling of (U-Th)/He ages of apatite and zircon defines three cooling pulses from Eocene to Miocene
19	Southern Snake Range	Miller et al. (1999)	>31 Ma	uncertain	Murphy Wash: normal faults that sole into NSRD are overlapped by 31 Ma tuff
20	Northern Schell Creek Range	Gans et al. (1989)	36–27.4 Ma	syn	Low-offset normal faults are syn- and post-36 Ma volcanism; early extension completed before 27.4 Ma

Table 3 *(continued)*

Number on Figure 11	Location	Data source	Extension timing	Timing relative to volcanism	Explanation of supporting data
21	Central Schell Creek Range	Druschke, Hanson, and Wells (2009)	36.5–35.9 Ma	syn	36.4 ± 0.1 Ma Cave Lake section of Kinsey Canyon Formation was tilted 30° prior to eruption of 36.0 ± 0.1 Ma rhyolite
22	Central Schell Creek Range	Druschke, Hanson, and Wells (2009)	35.5–35.2 Ma	syn	35.4 ± 0.1 Ma type section of Kinsey Canyon Formation was tilted 20° prior to eruption of 32.3 ± 0.1 Ma Kalamazoo tuff
23	Northern Egan Range	Gans and Miller (1983); Gans et al. (1989)	35.8 Ma	syn	Earliest extension in Hunter district during 35.8 Ma volcanism (ryholite dikes intrude and cut normal faults)
24	Central Egan Range	Gans et al. (2001)	37.6–36.7 Ma	syn	Rapid extension bracketed with 40Ar/39Ar ages of pre-, syn- and post-extensional volcanic rocks; Robinson district
25	Southern Egan Range	Druschke, Hanson, Wells, Rasbury, et al. (2009); Druschke, Hanson, and Wells (2009)	81.3–66.1 and 41–35.5 Ma	pre, overlaps	Sheep Pass Formation deposited in Late Cretaceous half graben; renewed slip in middle-late Eocene.
26	Southern Egan Range	Druschke, Hanson, and Wells (2009)	59.2–56.0 and 41–35.5 Ma	pre, overlaps	Upper Paleocene Sheep Pass Fm coarsens toward normal fault; late Eocene sediments tilted before 38–35.5 Ma volcanism
27	Condor Canyon, near Pioche	Axen et al. (1988)	~34–29.5 Ma	overlaps	Stampede detachment overlapped by tuffs as old as 29.5 Ma; motion on fault system interpreted as Oligocene
28	Ely Springs Range	Axen et al. (1988); Taylor et al. (1989)	~34–31.3 Ma	overlaps	Stampede detachment overlapped by tuffs as old as 31.3 Ma; motion on fault system interpreted as Oligocene
29	North Pahroc Range	Taylor et al. (1989)	30–27 Ma	syn	Syn-volcanic normal faults cut a 30 Ma tuff and are overlapped by a 27 Ma conglomerate
30	North Pahroc Range	Taylor and Bartley (1992); Axen et al. (1993)	36–31 Ma	overlaps	Early Oligocene fossils within syn-extensional formation of Rattlesnake Spring; overlain by ~31 Ma tuff.
31	Seaman Range	Taylor and Bartley (1992)	~34–30.6 Ma	pre	Breakaway of Stampede detachment overlapped by 30.6 Ma volcanics; motion on fault system interpreted as Oligocene
32	Central Grant Range	Long and Walker (2015)	32–29 Ma	overlaps	Initiation of extension on Grant Range detachment system post-dates 32 Ma volcanics and predates 29 Ma dike
33	Southern Grant Range	This study	31–15 Ma	overlaps	31–15 Ma rapid cooling of rocks exhumed by Grant Range detachment system; integrated with sequential reconstruction
34	Southern Grant Range	Fryxell (1988); Taylor et al. (1989)	28.2–22.6	overlaps	Troy Canyon fault cuts 27.8 ± 0.4 Ma tuff; 25.3 ± 0.5 Ma and 23.1 ± 0.5 Ma 40Ar/39Ar white mica cooling ages from Troy stockTroy Canyon fault cuts 27.8 ± 0.4 Ma tuff; 25.3 ± 0.5 Ma and 23.1 ± 0.5 Ma 40Ar/39Ar white mica cooling ages from Troy stock
35	Northern Quinn Canyon Range	Taylor et al. (1989)	31.8–27.3 Ma	overlaps	Normal faults cut 31.8 Windous Butte Formation and are cut by a 27.3 Ma felsite intrusion
36	Northern Quinn Canyon Range	Bartley and Gleason (1990)	32–26 Ma	overlaps	Wadsworth Ranch fault buts 32 Ma Windous Butte Fm, but is cut by 26–27 Ma felsite intrusion
37	Diamond Mtns./Fish Creek Range	Long et al. (2015)	75–60 Ma	pre	Late Cretaceous-Paleocene cooling histories interpreted as normal fault-related exhumation
38	Duckwater Mountains	Druschke, Hanson, and Wells (2009)	36.4–34.5 Ma	overlaps	Boulder fanglomerate within 35.7 ± 0.7 to 35.3 ± 0.8 Ma Sheep Pass Formation interpreted as synextensional deposits
39	Monitor Range	Kleinhampl and Ziony (1985); Axen et al. (1993)	>34–27 Ma	uncertain	Normal faults are overlapped by 34–27 Ma volcanic unit 'Twa'
40	Hot Creek Range	Quinlivan and Rogers (1974)	>27–31 Ma	uncertain	Normal faults overlapped by 31 Ma rhyolite flows and 27 Ma sedimentary rocks

Table 3 *(continued)*

Number on Figure 11	Location	Data source	Extension timing	Timing relative to volcanism	Explanation of supporting data
41	Northern Toiyabe Range	Smith (1992)	34–29 Ma	syn	Normal faults in northern Toiyabe Range initiated in earliest Oligocene, based on field relationships with tuffs
42	Central Toiyabe Range	Speed and McKee (1976); Kleinhampl and Ziony (1985)	54–22 Ma	uncertain	West-dipping normal fault predates 22 Ma volcanics and cuts 54 Ma pluton
43	Central Toiyabe Range	Speed and McKee (1976)	23 Ma	syn	High-angle normals faults cut by dikes correlated with a 23 Ma volcanic unit
44	Southern Toquima Range	John et al. (1989)	32–26 Ma	overlaps	At Round Mountain, earliest normal faults post-date ~32 Ma tuffs but predate 26 Ma mineralization
45	Southern Toquima Range	Boden (1986); Axen et al. (1993)	27–24 Ma	syn	Structural control and early normal faults during formation of ~27–24 Ma Toquima caldera complex
46	Southern Toiyabe Range	Brem et al. (1985); Axen et al. (1993)	25 Ma	syn	Structural control and early normal faults during formation of ~25 Ma Peavine caldera complex
47	Cedar Mountains	Hardyman et al. (1993)	27 Ma	syn	Earliest normal faulting at ~27 Ma, bracketed by pre- and post-faulting tuffs
48	Royston Hills	Seedorff (1991a)	27–20 Ma	syn	Earliest normal faulting bracketed by pre- and post-faulting ash flow tuffs
49	San Antonio Mountains	Shaver and McWilliams (1987)	24–17 Ma	syn	Earliest normal faults post-date ~24 Ma ash flow tuffs but predate ~17 Ma andesite flows
50	Tonopah area	Bonham and Garside (1979)	22–16 Ma	syn	Earliest normal faults post-date ~22 Ma ash flow tuffs but predate ~16 Ma andesite flows
51	Lone Mountain	Bonham and Garside (1979)	22–16 Ma	syn	Earliest normal faults post-date ~22 Ma ash flow tuffs but predate ~16 Ma andesite flows

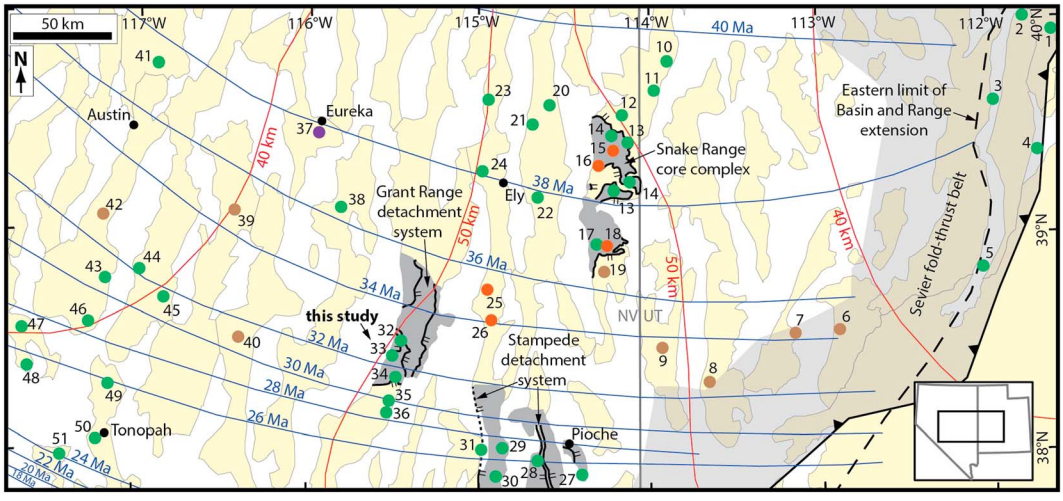

Figure 11. Compilation of published sites of late Eocene-Oligocene and older extension across central and eastern Nevada and west-central Utah (sites are referenced to Table 3). Blue lines are age contours of initial ignimbrite flare-up volcanism (from Henry & John, 2013), and red lines are contours of estimated pre-extensional crustal thickness (from Best et al., 2009; Coney & Harms, 1984). Range polygons are from McQuarrie and Wernicke (2005). Green sites are locations where extension is syn-volcanic or overlaps temporally with the regional sweep of volcanism. Orange sites are locations that underwent extension both prior to (Paleocene-middle Eocene) and during the late Eocene-Oligocene. Brown sites are locations of pre-volcanic extension with no lower age bound. Purple site represents a locality of Late Cretaceous-Paleocene extension. Major extensional fault systems that accommodated much or all of their overall motion during the late Eocene-Oligocene are labeled, and include the Grant Range and Stampede detachment systems and the Snake Range core complex.

Coney & Harms, 1984). Spatially isolated Late Cretaceous-Paleocene (~80–60 Ma) extension has been interpreted in four localities in eastern Nevada, and included upper-crustal normal faulting (Camilleri & Chamberlain, 1997; Druschke, Hanson, Wells, Rasbury, et al., 2009; Long et al., 2015) and initial exhumation of mid-crustal rocks in the Ruby-East Humboldt core complex (e.g., Hallett & Spear, 2014; McGrew et al., 2000). This syn-contractional extension is interpreted to have been triggered by thermal weakening and isostatic wedge adjustment that accompanied lithospheric delamination (Wells & Hoisch, 2008).

During and after the terminal stages of Sevier shortening, eastward migration of crustal shortening and magmatism during Paleocene-early Eocene (~65–45 Ma) construction of the Laramide province is interpreted as a consequence of shallowing of the subducting Farallon slab (e.g., Dickinson & Snyder, 1978; Dickinson, 2004; Saleeby, 1993; Yonkee & Weil, 2015). On the area of Figure 11 (and in proximal areas to the north), extension of this age is documented in only four places, including normal faulting in the Egan Range in eastern Nevada (Druschke, Hanson, & Wells, 2009) and the Deep Creek Range in western Utah (Potter et al., 1995), normal faulting and continued exhumation in the Ruby-East Humboldt core complex (Camilleri & Chamberlain, 1997; McGrew et al., 2000), and initial exhumation in the Snake Range (Evans et al., 2015; Gébelin et al., 2014; Lee, 1995).

Following Laramide deformation, the Great Basin ignimbrite flare-up swept from NE to SW across Nevada between the late Eocene and Oligocene (~42–24 Ma; Figures 1 and 11; e.g., Armstrong & Ward, 1991; Best et al., 2009; Henry & John, 2013). This sweep of volcanism has been interpreted as the result of steepening of the subduction angle of the Farallon slab (e.g., Dickinson, 2002; Humphreys, 1995). During this time, the Cordilleran plateau experienced its first episode of spatially distributed extension. On the area of Figure 11, at least 41 localities record late Eocene-Oligocene extension, with some sites that experienced demonstrably syn-volcanic extension, and others that record extension that overlaps broadly in time with the sweep of volcanism through the region. Extension accommodated in these localities was highly variable in style and magnitude, ranging in scale from single normal faults (e.g., Constenius, 1996; Taylor et al., 1989) to high-strain, regional-scale normal fault systems (e.g., Axen et al., 1988; Gans & Miller, 1983; this study). The Grant Range detachment system, along with the Snake Range core complex and Stampede detachment system, represent three regional-scale fault systems on the area of Figure 11 that accommodated much or all of their overall motion during the late Eocene-Oligocene. In the Snake Range, denudation-related cooling of footwall rocks and dated field relations with volcanic, intrusive and sedimentary rocks defines a protracted history of extension that spans from the early Eocene to the middle Miocene (Evans et al., 2015; Gans et al., 1989; Gébelin et al., 2014; Lee & Sutter, 1991; Lee, 1995; Lee et al., 2017; Miller et al., 1999). The Stampede detachment system was active during deposition of ~34–31 Ma sedimentary rocks and prior to ~29–31 Ma volcanism (Axen et al., 1988, 1993; Bartley et al., 1988; Taylor, 1990; Taylor & Bartley, 1992). In this study, we demonstrate that the Grant Range detachment system was active from ~28–31 to ~15–19 Ma.

Several studies have reviewed the space-time patterns of extension and ignimbrite flare-up volcanism (Axen et al., 1993; Best & Christiansen, 1991; Best et al., 2009; Druschke, Hanson, & Wells, 2009; Gans et al., 1989; Glazner & Supplee, 1982; John et al., 1989; Seedorff, 1991b; Taylor & Bartley, 1992). Although syn-volcanic extension is documented in several localities (e.g., Gans et al., 1989, 2001; Taylor et al., 1989), several of these studies have concluded that there was no direct, regional space-time association between the initiation of extension and proximal volcanism (Axen et al., 1993; Best & Christiansen, 1991; Dickinson, 2002, 2006). However, when viewed in the larger geodynamic context of post-Laramide slab rollback, this episode of late Eocene-Oligocene extension illuminates the role of deeper-seated geodynamic processes in driving extension. Several processes, either acting independently or in concert, can be invoked for activating late Eocene-Oligocene extension, including (1) gravitational potential energy generated by gradients in crustal thickness between eastern Nevada and the surrounding regions, which would promote lateral spreading (e.g., Coney & Harms, 1984; Dewey, 1988; Sonder et al., 1987; Sonder & Jones, 1999); and (2) processes associated with slab rollback, including a decrease in interplate coupling, trench retreat, and advective heating of the crust as a result of asthenospheric upwelling (e.g., Dickinson, 1991, 2002; Humphreys, 1995). The coincidence in timing between slab rollback and the earliest spatially distributed extensional episode recorded in the Cordilleran plateau implies that rollback served as the dominant triggering mechanism. This indicates that external geodynamic driving mechanisms, including slab rollback in the case of late Eocene-Oligocene extension, and reorganization of the Pacific-North American plate boundary in the case

of Neogene Basin and Range extension, were necessary to activate major extensional episodes. Therefore, though crust thickened during Cordilleran orogenesis was a precondition that dictated the spatial extent of Cenozoic extension (e.g., Dickinson, 2002), external geodynamic events, including slab rollback and the demise of subduction, were the primary drivers of extensional episodes. This illuminates a scenario of orogenic collapse proceeding in distinct episodes that were initiated by abrupt changes in boundary conditions, as opposed to gradual gravitational spreading.

7. Conclusions

1. A set of down-to-west, brittle detachment faults in the Grant Range accommodated ~24 km of extension (~115%), and exhumed granite and greenschist-facies metasedimentary rocks from depths of ~7–9 to ~1–1.5 km. Muscovite $^{40}Ar/^{39}Ar$ MDD modeling and fission track and (U-Th)/He ages from zircon and apatite collected from exhumed granite samples define rapid cooling (20–35 °C/Myr) from 350–425 to 25–50 °C between 28–31 and 15–19 Ma. This episode of rapid cooling is interpreted to date the duration of motion on the detachment system and defines a long-term extension rate of 1.5–2.6 km/Myr.
2. The Grant Range fault system can be placed in the context of late Eocene-Oligocene extension of thickened Cordilleran crust during post-Laramide slab rollback, and was one of the most regionally significant and highest-strain fault systems active during this time. Upper-crustal extension, though variable in style and magnitude, was distributed across a large area of Nevada and Utah during the late Eocene-Oligocene. The timing of the Grant Range detachment system provides further support that the decrease in interplate coupling that accompanied slab rollback was likely the primary driver of the earliest episode of distributed extension within the Cordilleran plateau during the final stages of subduction. When combined with the documented phase of Neogene 'Basin and Range' extension that was triggered by plate boundary reorganization, this illustrates that collapse of the Cordillera proceeded in distinct episodes that were initiated by changes in boundary conditions.

References in Supporting Information

These references contributed to the supporting files: Brandon et al. (1998), Cebull (1970), Galbraith (2005), Galbraith and Laslett (1993), Gleadow (1981), Gleadow et al. (1976), Guenthner et al. (2013), Hurford (1990), Hurford and Green (1983), Ketcham et al. (2007a), Ketcham et al. (2007b), Ketcham et al. (2011), Kuiper et al. (2008), Leeder and Gawthorpe (1987), Ludwig (2008), McDowell et al. (2005), Min et al. (2000), Rahn et al. (2004), Reiners (2005), Sanders et al. (2006), Schmitz and Bowring (2001), Shuster et al. (2006), Steiger and Jäger (1977), Taylor (1982), and Yamada et al. (2007).

Acknowledgments
Makoil, Inc. (CEO Gregg Kozlowski) generously supported this project. Ryan Anderson performed mineral separation, Jerome Walker provided advice on oil well log interpretation, and Uttam Chowdhury provided assistance at the Arizona Radiogenic Helium Dating Laboratory. Conversations with Chris Henry, Sue Beard, Karen Lund, Jim Faulds, and Phyllis Camilleri inspired several aspects of this work. This paper was improved by constructive reviews from two anonymous reviewers, associate editor Luc Lavier, and editor John Geissman. The manuscript and supporting information contain all of the data used for this research.

References

Allmendinger, R. W. (1992). Fold and thrust tectonics of the western United States exclusive of the accreted terranes. In B. C. Burchfiel, et al. (Eds.), *The Cordilleran Orogen: Conterminous U.S*, *Geol. North Amer.* (Vol. G-3, pp. 583–607). Boulder, CO: Geol. Soc. Amer.

Armstrong, R. L. (1970). Geochronology of Tertiary igneous rocks, eastern Basin and Range province, western Utah, eastern Nevada, and vicinity, U.S.A. *Geochimica et Cosmochimica Acta*, *34*, 203–232.

Armstrong, R. L. (1972). Low-angle (denudation) faults, hinterland of the Sevier orogenic belt, eastern Nevada and western Utah. *Geological Society of America Bulletin*, *83*(6), 1729–1754. https://doi.org/10.1130/0016-7606(1972)83[1729:LDFHOT]2.0.CO;2

Armstrong, R. L., & Ward, P. (1991). Evolving geographic patterns of Cenozoic magmatism in the North American Cordillera: The temporal and spatial association of magmatism and metamorphic core complexes. *Journal of Geophysical Research*, *96*(B8), 13,201–13,224. https://doi.org/10.1029/91JB00412

Atwater, T. (1970). Implications of plate tectonics for the Cenozoic evolution of North America. *Geological Society of America Bulletin*, *81*(12), 3513–3536. https://doi.org/10.1130/0016-7606(1970)81[3513:IOPTFT]2.0.CO;2

Axen, G. J., Lewis, K. J., Burke, K. J., Sleeper, K. G., & Fletcher, J. M. (1988). Tertiary extension in the Pioche Area, Nevada. In D. L. Weide & M. L. Faber (Eds.), *This extended land, geological journeys in the southern Basin and Range*, *Cordilleran Section Field trip Guidebook* (pp. 3–5). Las Vegas, NV: Geological Society of America.

Axen, G. J., Taylor, W. J., & Bartley, J. M. (1993). Space-time patterns and tectonic controls of Tertiary extension and magmatism in the Great Basin of the western United States. *Geological Society of America Bulletin*, *105*(1), 56–76. https://doi.org/10.1130/0016-7606(1993)105<0056:STPATC>2.3.CO;2

Baldwin, S. L., & Harrison, T. M. (1989). Geochronology of blueschists for west-central Baja California and the timing of uplift in subduction complexes. *Journal of Geology*, *97*(2), 149–163. https://doi.org/10.1086/629291

Bartley, J. M., Fryxell, J. E., Murray, M. E., & Wright, S. D. (1984). Patterns of tertiary extension in the Great Basin exemplified in the Grant/Quinn Canyon Range, Nevada. Geol. Soc. Amer. Abstr. Prog., 16, 438.

Bartley, J. M., Axen, G. J., Taylor, W. J., & Fryxell, J. E. (1988). Cenozoic tectonics of a transect through eastern Nevada near 38°N latitude. In D. L. Weide & M. L. Faber (Eds.), *This extended land, geological journeys in the Southern Basin and Range*, *Cordilleran section field trip guidebook* (pp. 1–20). Las Vegas, NV: Geological Society of America.

Bartley, J. M., & Gleason, G. C. (1990). Tertiary normal faults superimposed on Mesozoic thrusts, Quinn Canyon and Grant Ranges, Nye County, Nevada. In B. P. Wernicke (Ed.), *Basin and range extensional tectonics near the latitude of Las Vegas Nevada*, *Mem. Geol. Soc. Amer.* (Vol. 176, pp. 195–212). Boulder, CO: Geological Society of America.

Bernet, M. (2009). A field-based estimate of the zircon fission-track closure temperature. *Chemical Geology*, *259*, 181–189. https://doi.org/10.1016/j.chemgeo.2008.10.043

Best, M. G., Barr, D. L., Christiansen, E. H., Gromme, S., Deino, A. L., & Tingey, D. G. (2009). The Great Basin Altiplano during the middle Cenozoic ignimbrite flareup: Insights from volcanic rocks. *International Geology Review*, *51*, 589–633. https://doi.org/10.1080/00206810902867690

Best, M. G., & Christiansen, E. H. (1991). Limited extension during peak Tertiary volcanism, Great Basin of Nevada and Utah. *Journal of Geophysical Research*, *96*, 13,509–13,528. https://doi.org/10.1029/91JB00244

Boden, D. R. (1986). Eruptive history and structural development of the Toquima caldera complex, central Nevada. *Geological Society of America Bulletin*, *101*, 1076–1090.

Bonham, H. F. Jr., & Garside, L. J. (1979). Geology of the Tonopah, Lone Mountain, Klondike, and northern Mud Lake quadrangles, Nevada. *Bulletins of the Nevada Bureau of Mines and Geology*, *92*, 142.

Brandon, M. T., Roden-Tice, M. K., & Garver, J. I. (1998). Late Cenozoic exhumation of the Casdacia accretionary wedge in the Olympic Mountains, northwest Washington State. *Geological Society of America Bulletin*, *110*, 985–1009.

Brem, G. F., Purdy, T. L., & Snyder, D. B. (1985). Oligocene and Miocene volcanic-tectonic history of the southern Toiyabe and Shoshone Mountains, Nevada. Geol. Soc. Amer. Abstr. Prog., 17, 343.

Burchfiel, B. C., & Royden, L. H. (1985). North-south extension within the convergent Himalayan region. *Geology*, *13*, 679–682.

Camilleri, P. A. (2013). Geologic map and structure of the west-central part of the Grant Range, Nye County, Nevada. Geol. Soc. Amer. Dig. Map Chart Ser., 14 (25 pp.). https://doi.org/10.1130/2013.DMCH014

Camilleri, P. A., & Chamberlain, K. R. (1997). Mesozoic tectonics and metamorphism in the Pequop Mountains and Wood Hills region, northeast Nevada: Implications for the architecture and evolution of the Sevier orogeny. *Geological Society of America Bulletin*, *109*, 74–94. https://doi.org/10.1130/0016-7606(1997)109<0074:MTAMIT>2.3.CO;2

Cassel, E. J., Breecker, D. O., Henry, C. D., Larson, T. E., & Stockli, D. F. (2014). Profile of a paleo-orogen: High topography across the present-day Basin and Range from 40 to 23 Ma. *Geology*, *42*, 1007–1010. https://doi.org/10.1130/G35924.1

Cebull, S. E. (1970). Bedrock geology and orogenic succession in southern Grant Range, Nye County, Nevada. *American Association of Petroleum Geologists Bulletin*, *54*, 1828–1842.

Chapman, J. B., Ducea, M. N., DeCelles, P. G., & Profeta, L. (2015). Tracking changes in crustal thickness during orogenic evolution with Sr/Y: An example from the North American Cordillera. *Geology*, *43*, 919–922. https://doi.org/10.1130/G36996.1

Coleman, D. S., & Walker, J. D. (1990). Generation of juvenile granitic crust during continental extension: A case study from the Mineral Mountains batholith, Utah. *Eos, Transactions American Geophysical Union*, *71*, 1682.

Colgan, J. P., Dumitru, T. A., Reiners, P. W., Wooden, J. L., & Miller, E. L. (2006). Cenozoic tectonic evolution of the Basin and Range Province in northwestern Nevada. *American Journal of Science*, *306*, 616–654. https://doi.org/10.2475/08.2006.02

Colgan, J. P., & Henry, C. D. (2009). Rapid middle Miocene collapse of the Sevier orogenic plateau in north-central Nevada. *International Geology Review*, *51*, 920–961. https://doi.org/10.1080/00206810903056731

Coney, P. J., & Harms, T. J. (1984). Cordilleran metamorphic core complexes: Cenozoic extensional relics of Mesozoic compression. *Geology*, *12*, 550–554. https://doi.org/10.1130/0091-7613(1984)12<550:CMCCCE>2.0.CO;2

Constenius, K. N. (1996). Late Paleogene extensional collapse of the Cordilleran foreland fold and thrust belt. *Geological Society of America Bulletin*, *108*, 20–39. https://doi.org/10.1130/0016-7606(1996)108<0020:LPECOT>2.3.CO;2

Cooper, F. J., Platt, J. P., Anczkiewicz, R., & Whitehouse, M. J. (2010). Footwall dip of a core complex detachment fault: Thermobarometric constraints from the northern Snake Range (Basin and Range, USA). *Journal of Metamorphic Geology*, *28*, 997–1020. https://doi.org/10.1111/j.1525-1314.2010.00907.x

Dallmeyer, R. D., & Villeneuve, M. (1987). $^{40}Ar/^{39}Ar$ mineral age record of polyphase tectonothermal evolution in the southern Mauritanide orogeny, southeastern Senegal. *Geological Society of America Bulletin*, *98*, 602–611.

Dalmayrac, B., & Molnar, P. (1981). Parallel thrust and normal faulting in Peru and the constraints on the state of stress. *Earth and Planetary Science Letters*, *55*, 473–481. https://doi.org/10.1016/0012-821X(81)90174-6

Davis, G. A., & Lister, G. S. (1988). Detachment faulting in continental extension: Perspectives from the southwestern U.S. Cordillera. In S. P. Clark (Ed.), *Processes in continental lithospheric deformation*, *Geol. Soc. Amer. Spec. Pap.* (Vol. 218, pp. 133–159). Boulder, CO: Geological Society of America.

DeCelles, P. G. (2004). Late Jurassic to Eocene evolution of the Cordilleran thrust belt and foreland basin system, western U.S.A. *American Journal of Science*, *304*, 105–168. https://doi.org/10.2475/ajs.304.2.105

DeCelles, P. G., & Coogan, J. C. (2006). Regional structure and kinematic history of the Sevier fold-and-thrust belt, central Utah. *Geological Society of America Bulletin*, *118*, 841–864. https://doi.org/10.1130/B25759.1

Dewey, J. F. (1988). Extensional collapse of orogens. *Tectonics*, *7*, 1123–1139.

Dickinson, W. R. (1991). Tectonic setting of faulted Tertiary strata associated with the Catalina core complex in southern Arizona. *Geological Society of America Special Papers*, *264*, 106.

Dickinson, W. R. (1997). Tectonic implications of Cenozoic volcanism in coastal California. *Geological Society of America Bulletin*, *109*, 936–954.

Dickinson, W. R. (2002). The Basin and Range province as a composite extensional domain. *International Geology Review*, *44*, 1–38. https://doi.org/10.2747/0020-6814.44.1.1

Dickinson, W. R. (2004). Evolution of the North American Cordillera. *Annual Review of Earth and Planetary Sciences*, *32*, 13–45. https://doi.org/10.1146/annurev.earth.32.101802.120257

Dickinson, W. R. (2006). Geotectonic evolution of the Great Basin. *Geosphere*, *2*, 353–368. https://doi.org/10.1130/GES00054.1

Dickinson, W. R., & Snyder, W. S. (1978). Plate tectonics of the Laramide orogeny. In V. Mathews, III (Ed.), *Laramide folding associated with basement block faulting in the Western United States*, *Geol. Soc. Amer. Mem.* (Vol. 151, pp. 355–366). Boulder, CO: Geological Society of America.

Dilek, Y., & Moores, E. M. (1999). A Tibetan model for the early Tertiary western United States. *Journal of the Geological Society of London*, *156*, 929–941.

Dixon, G. L., Hedlund, D. C., & Ekren, E. B. (1972). Geologic map of the Pritchards Station quadrangle, Nye County, Nevada. USGS Misc. Geol. Invest. Map I-728.

Druschke, P., Hanson, A. D., & Wells, M. L. (2009). Structural, stratigraphic, and geochronologic evidence for extension predating Palaeogene volcanism in the Sevier hinterland, east-central Nevada. *International Geology Review*, *51*, 743–775. https://doi.org/10.1080/00206810902917941

Druschke, P., Hanson, A. D., Wells, M. L., Rasbury, T., Stockli, D. F., & Gehrels, G. (2009). Synconvergent surface-breaking normal faults of Late Cretaceous age within the Sevier hinterland, east-central Nevada. *Geology*, *37*, 447–450. https://doi.org/10.1130/G25546A.1

Effimoff, I., & Pinezich, A. R. (1981). Tertiary structural development of selected valleys based on seismic data, Basin and Range Province, northeastern Nevada. In *Extensional tectonics associated with convergent plate boundaries*, *Philosophical Transactions of the Royal Society A: Mathematical, Physical and Engineering* (Vol. 300, pp. 435–442). London: Royal Society.

Ekren, E. B., Hinrichs, E. N., & Dixon, G. L. (1972). Geologic map of the Wall quadrangle, Nye County, Nevada. USGS Misc. Geol. Invest. Map I-719.

Ekren, E. B., Hinrichs, E. N., Quinlivan, W. D., & Hoover, D. L. (1973). Geologic map of the Moores Station quadrangle, Nye County, Nevada. USGS Misc. Geol. Invest. Map I-756.

Ekren, E. B., Rogers, C. L., & Dixon, G. L. (1973). Geologic and Bouguer gravity map of the Reveille quadrangle, Nye County, Nevada. USGS Misc. Invest. Ser. Map I-806.

Elliott, D. (1983). The construction of balanced cross-sections. *Journal of Structural Geology*, *5*, 101.

Evans, S. L., Styron, R. H., van Soest, M. C., Hodges, K. V., & Hanson, A. D. (2015). Zircon and apatite (U-Th)/He evidence for Paleogene and Neogene extension in the Southern Snake Range, Nevada, USA. *Tectonics*, *34*, 2142–2164. https://doi.org/10.1002/2015TC003913

Faulds, J. E., & Henry, C. D. (2008). Tectonic influences on the spatial and temporal evolution of the Walker Lane: An incipient transform fault along the evolving Pacific–North American plate boundary. In J. E. Spencer & S. R. Titley (Eds.), *Ores and orogenesis: Circum-Pacific tectonics, geologic evolution, and ore deposits*, *Ariz. Geol. Soc. Dig.* (Vol. 22, pp. 437–470). Tucson, AZ: Arizona Geological Society.

Flowers, R. M., Ketcham, R. A., Shuster, D. L., & Farley, K. A. (2009). Apatite (U–Th)/He thermochronometry using a radiation damage accumulation and annealing model. *Geochimica et Cosmochimica Acta*, *73*, 2347–2365.

Forster, T. M., & Lister, G. S. (2014). $^{40}Ar/^{39}Ar$ geochronology and the diffusion of ^{39}Ar in phengite–muscovite intergrowths during step-heating experiments in vacuo. In F. Jourdan, D. F. Mark, & C. Verati (Eds.), *Advances in $^{40}Ar/^{39}Ar$ dating: From archeology to planetary sciences*, *Special Publications* (Vol. 378, pp. 117–135). London: Geological Society. https://doi.org/10.1144/SP378.16

Foster, D. A., Gleadow, A. J. W., Reynolds, S. J., & Fitzgerald, P. G. (1993). Denudation of metamorphic core complexes and the reconstruction of the transition zone, west-central Arizona: Constraints from apatite fission track thermochronology. *Journal of Geophysical Research*, *98*, 2167–2185. https://doi.org/10.1029/92JB02407

Friedrich, A., & Bartley, J. M. (1992). Mid-Tertiary prevolcanic extension in the southern Wah Wah Mountains, SW Utah. Geol. Soc. Amer. Abstr. Prog., Women in Geoscience Conference (pp. 6–7).

Fryxell, J. E. (1984). Structural development of the west-central Grant Range, Nye County, Nevada (PhD dissertation, pp. 139). Chapel Hill: University of North Carolina.

Fryxell, J. E. (1988). Geologic map and description of stratigraphy and structure of the west-central Grant Range, Nye County, Nevada. Geol. Soc. Amer. Map Chart Ser. MCH064 (16 pp.).

Fryxell, J. E. (1991). Tertiary tectonic denudation of an igneous and metamorphic complex, west-central Grant Range, Nye County, Nevada. In *Geology and ore deposits of the Great Basin symposium* (pp. 87–92). Reno, NV: Geol. Soc. Nevada.

Galbraith, R. F. (2005). *Statistics for fission track analysis* (p. 219). Boca Raton, FL: Chapman & Hall/CRC.

Galbraith, R. F., & Laslett, G. M. (1993). Statistical models for mixed fission track ages. *Nuclear Tracks*, *21*, 459–470.

Gans, P. B., Mahood, G. A., & Schermer, E. (1989). Synextensional magmatism in the Basin and Range Province: A case study from the eastern Great Basin. *Geological Society of America Special Papers*, *223*, 53.

Gans, P. B., & Miller, E. L. (1983). Style of mid-Tertiary extension in east-central Nevada. In K. D. Gurgel (Ed.), *Geologic excursions in the overthrust belt and metamorphic core complexes of the Intermountain Region*, *Utah Geol. Min. Surv. Spec. Stud.* (Vol. 59, pp. 107–160). Salt Lake City, UT: Utah Geological and Mineral Survey.

Gans, P. B., Miller, E. L., Brown, R., Houseman, G., & Lister, G. S. (1991). Assessing the amount, rate and timing of tilting in normal fault blocks: A case study of tilted granites in the Kern–Deep Creek Mountains, Utah. Geol. Soc. Amer. Abstr. Prog., 23 (p. 28).

Gans, P. B., Miller, E. L., McCarthy, J., & Oldcott, M. L. (1985). Tertiary extensional faulting and evolving ductile-brittle transition zones in the northern Snake Range and vicinity: New insights from seismic data. *Geology*, *13*, 189–193.

Gans, P. B., Seedorff, E., Fahey, P. L., Hasler, R. W., Maher, D. J., Jeanne, R. A., & Shaver, S. A. (2001). Rapid Eocene extension in the Robinson district, White Pine County, Nevada: Constraints from $^{40}Ar/^{39}Ar$ dating. *Geology*, *29*, 475–487.

Gébelin, A., Teyssier, C., Heizler, M., & Mulch, A. (2014). Meteoric water circulation in a rolling-hinge detachment system (northern Snake Range core complex, Nevada). *Geological Society of America Bulletin*, *127*, 149–161. https://doi.org/10.1130/B31063.1

Glazner, A. F., & Supplee, J. A. (1982). Migration of Tertiary volcanism in the southwestern United States and subduction of the Mendocino fracture zone. *Earth and Planetary Science Letters*, *60*, 429–436.

Gleadow, A. J. W. (1981). Fission-track dating methods: What are the real alternatives? *Nuclear Tracks*, *5*, 3–14.

Gleadow, A. J.W., Hurford, A. J., & Quaife, R. D. (1976). Fission track dating of zircon: Improved etching techniques. *Earth and Planetary Science Letters*, *33*, 273–276.

Guenthner, W. R., Reiners, P. W., Ketcham, R. A., Nasdala, L., & Geister, G. (2013). Helium diffusion in natural zircon: Radiation damage, anisotropy, and the interpretation of zircon (U-Th)/He thermochronology. *American Journal of Science*, *313*, 145–198. https://doi.org/10.2475/03.2013.01

Hallett, B. W., & Spear, F. S. (2014). The P-T History of anatectic pelites of the northern East Humboldt Range, Nevada: evidence for tectonic loading, decompression, and anatexis. *Journal of Petrology*, *55*, 3–36. https://doi.org/10.1093/petrology/egt057

Hardyman, R. F., McKee, E. H., Snee, L. W., & Whitebread, D. H. (1993). The Camp Terrill and Dicalite Summit faults: Two contrasting examples of detachment faults in the central Walker Lane. In S. D. Craig (Ed.), *Structure, tectonics and mineralization of the Walker Lane*, *Walker Lane Sympos. Proceed.* (pp. 93–113). Reno, NV: Geol. Soc. Nevada.

Harrison, T. M., Celerier, J., Aikman, A. B., Hermann, J., & Heizler, M. T. (2009). Diffusion of ^{40}Ar in muscovite. *Geochimica et Cosmochimica Acta*, *73*, 1039–1051. https://doi.org/10.1016/j.gca.2008.09.038

Harrison, T. M., & Lovera, O. M. (2013). The multi-diffusion domain model: Past, present and future. In F. Jourdan, D. F. Mark, & C. Verati (Eds.), *Advances in $^{40}Ar/^{39}Ar$ dating: From archaeology to planetary sciences*, *Special Publications* (Vol. 378, pp. 91–106). London: Geological Society. https://doi.org/10.1144/SP378.9

Heizler, M. T. (1994). Muscovite $^{40}Ar/^{39}Ar$ age gradients and the age of low-temperature deformation: An experimental approach. Geol. Soc. Amer. Abstr. Prog., 528, 143.

Heizler, M. T., & Harrison, T. M. (2009). Continuous thermal histories from muscovite $^{40}Ar/^{39}Ar$ age spectra. Goldschmidt conference abstracts, June 21–26, Davos Switzerland.

Heizler, M. T., Ralser, S., & Karlstrom, K. E. (1997). Late Proterozoic (Grenville?) deformation in central New Mexico determined from single crystal muscovite $^{40}Ar/^{39}Ar$ age spectra. *Precambrian Research*, *84*, 1–15.

Henry, C. D., & John, D. A. (2013). Magmatism, ash-flow tuffs, and calderas of the ignimbrite flareup in the western Nevada volcanic field, Great Basin, USA. *Geosphere*, *9*, 951–1008. https://doi.org/10.1130/GES00867.1

Henry, C. D., McGrew, A. J., Colgan, J. P., Snoke, A. W., & Brueseke, M. E. (2011). Timing, distribution, amount, and style of Cenozoic extension in the northern Great Basin. In J. Lee & J. P. Evans (Eds.), *Geologic field trips to the Basin and Range, Rocky Mountains, Snake River Plain, and Terranes of the U.S. Cordillera*, *Geol. Soc. Amer. Field Guide* (Vol. 21, pp. 27–66). Boulder, CO: Geological Society of America.

Hess, R. H., Fitch, S. P., & Warren, S. N. (2004). Nevada oil and gas well database. Nev. Bur. Mines Geol. Open-File Rep., 04–1.

Hodges, K. V., & Walker, J. D. (1992). Extension in the Cretaceous Sevier orogen, North American Cordillera. *Geological Society of America Bulletin*, *104*, 560–569. https://doi.org/10.1130/0016-7606(1992)104 < 0560:EITCSO>2.3.CO;2

Horton, B. K., & Schmitt, J. G. (1998). Development and exhumation of a Neogene sedimentary basin during extension, east-central Nevada. *Geological Society of America Bulletin*, *110*, 163–172.

Hourigan, J. K., Reiners, P. W., & Brandon, M. T. (2005). U-Th zonation-dependent alpha-ejection in (U-Th)/He chronometry. *Geochimica et Cosmochimica Acta*, *69*, 3349–3365.

Hulen, J. B., Goff, F., Ross, J. R., Bortz, L. C., & Bereskin, S. R. (1994). Geology and geothermal origin of Grant Canyon and Bacon Flat oil fields, Railroad Valley, Nevada. *American Association of Petroleum Geologists Bulletin*, *78*, 596–623.

Humphreys, E. D. (1995). Post-Laramide removal of the Farallon slab, western United States. *Geology*, *23*, 987–990.

Hurford, A. J. (1990). Standardization of fission track dating calibration: Recommended by the Fission Track Working Group of the I.U.G.S. Subcommission on Geochronology. *Chemical Geology*, *80*, 171–178.

Hurford, A. J., & Green, P. F. (1983). The Zeta age calibration of fission-track dating. *Isotope Geoscience*, *1*, 285–317.

Hyde, J. H., & Huttrer, G. W. (1970). Geology of the central Grant Range, Nevada. *American Association of Petroleum Geologists Bulletin*, *54*, 503–521.

John, D. A., Thomason, R. E., & McKee, E. H. (1989). Geology and K-Ar geochronology of the Paradise Peak Mine and the relationship of Pre-Basin and Range Extension to Early Miocene precious metal mineralization in West-Central Nevada. *Economic Geology*, *84*, 631–649.

Johnson, E. H. (1993). A look at Bacon Flat, Grant Canyon oil fields of Railroad Valley, Nevada. *Oil and Gas Journal*, *91*, 64–68.

Ketcham, R. A. (1996). Thermal models of core-complex evolution in Arizona and New Guinea: Implications for ancient cooling paths and present-day heat flow. *Tectonics*, *15*, 933–951.

Ketcham, R. A. (2005). Forward and inverse modeling of low-temperature thermochronometry data. In P. W. Reiners & T. A. Ehlers (Eds.), *Low-temperature thermochronology: Techniques, interpretations, and applications*, *Rev. Mineral. Geochem.* (Vol. 58, pp. 275–314). Chantilly, VA: Mineralogical Society of America.

Ketcham, R. A., Carter, A., Donelick, R. A., Barbarand, J., & Hurford, A. J. (2007a). Improved measurement of fission-track annealing in apatite using c-axis projection. *American Mineralogist*, *92*, 789–798. https://doi.org/10.2138/am.2007.2280

Ketcham, R. A., Carter, A., Donelick, R. A., Barbarand, J., & Hurford, A. J. (2007b). Improved modeling of fission-track annealing in apatite. *American Mineralogist*, *92*, 799–810. https://doi.org/10.2138/am.2007.2281

Ketcham, R. A., Gautheron, C., & Tassan-Got, L. (2011). Accounting for long alpha-particle stopping distances in (U-Th-Sm)/He geochronology: Refinement of the baseline case. *Geochimica et Cosmochimica Acta*, *75*, 7779–7791.

Kleinhampl, F. J., & Ziony, J. L. (1985). Geology of northern Nye County, Nevada. *Bulletins of the Nevada Bureau of Mines and Geology*, *99A*, 171.

Kuiper, K. F., Deino, A., Hilgen, F. J., Krijgsman, W., Renne, P. R., & Wijbrans, J. R. (2008). Synchronizing the rock clocks of Earth history. *Science*, *320*, 500–504.

Lee, J. (1995). Rapid uplift and rotation of mylonitic rocks from beneath a detachment fault: Insights from potassium feldspar $^{40}Ar/^{39}Ar$ thermochronology, northern Snake Range, Nevada. *Tectonics*, *14*, 54–77. https://doi.org/10.1029/94TC01508

Lee, J., Blackburn, T., & Johnston, S. (2017). Timing of mid-crustal ductile extension in the northern Snake Range metamorphic core complex, Nevada: Evidence from U/Pb zircon ages. *Geosphere*, *13*, 439–459. https://doi.org/10.1130/GES01429.1

Lee, J., & Sutter, J. F. (1991). Incremental $^{40}Ar/^{39}Ar$ thermochronology of mylonitic rocks from the northern Snake Range, Nevada. *Tectonics*, *10*, 77–100. https://doi.org/10.1029/90TC01931

Leeder, M. R., & Gawthorpe, R. L. (1987). Sedimentarymodels for extensional tilt-block/half-graben basins. In M. P. Coward, J. F. Dewey, & P. L. Hancock (Eds.), *Continental extensional tectonics*, *Geol. Soc. Am. Spec. Publ.* (Vol. 28, pp. 139–152). Boulder, CO: Geological Society of America.

Lemmon, D. M., & Morris, H. T. (1984). Geologic map of the Beaver Lake Mountains quadrangle, Millard and Beaver Counties, Utah. U.S.G.S. Misc. Invest. Map I-1572.

Lewis, C. J., Wernicke, B. P., Selverstone, J., & Bartley, J. M. (1999). Deep burial of the footwall of the northern Snake Range decollement, Nevada. *Geological Society of America Bulletin*, *111*, 39–51.

Long, S. P. (2012). Magnitudes and spatial patterns of erosional exhumation in the Sevier hinterland, eastern Nevada and western Utah, U.S.A.: Insights from a Paleogene paleogeologic map. *Geosphere*, *8*, 881–901. https://doi.org/10.1130/GES00783.1

Long, S. P. (2014). Preliminary geologic map of Heath Canyon, central Grant Range, Nye County, Nevada. Nev. Bur. Mines Geol. Open-File Rep. 14-6, scale 1:24,000 (4 p.).

Long, S. P. (2015). An upper-crustal fold province in the hinterland of the Sevier orogenic belt, eastern Nevada, U.S.A.: a Cordilleran Valley and Ridge in the Basin and Range. *Geosphere*, *11*, 404–424. https://doi.org/10.1130/GES01102.1

Long, S. P., Henry, C. D., Muntean, J. L., Edmondo, G. P., & Cassel, E. J. (2014). Early Cretaceous construction of a structural culmination, Eureka, Nevada, U.S.A.: Implications for out-of-sequence deformation in the Sevier hinterland. *Geosphere*, *10*, 564–584. https://doi.org/10.1130/GES00997.1

Long, S. P., & Soignard, E. (2016). Shallow-crustal metamorphism during Late Cretaceous anatexis in the Sevier hinterland plateau: Peak temperature conditions from the Grant Range, eastern Nevada, U.S.A. *Lithosphere*, *8*, 150–164. https://doi.org/10.1130/L501.1

Long, S. P., Thomson, S. N., Reiners, P. W., & Di Fiori, R. V. (2015). Synorogenic extension localized by upper-crustal thickening: An example from the Late Cretaceous Nevadaplano. *Geology*, *43*, 351–354. https://doi.org/10.1130/G36431.1

Long, S. P., & Walker, J. P. (2015). Geometry and kinematics of the Grant Range brittle detachment system, eastern Nevada, U.S.A.: An end-member style of upper-crustal extension. *Tectonics*, *34*, 1837–1862. https://doi.org/10.1002/2015TC003918

Lovera, O. M., Heizler, M. T., & Harrison, T. M. (1993). Argon diffusion domains in K-feldspar II: Kinetic properties of MH-10 K-feldspar. *Contributions to Mineralogy and Petrology*, *113*, 381–393.

Lovera, O. M., Richter, F. M., & Harrison, T. M. (1989). The $^{40}Ar/^{39}Ar$ geothermometry for slowly cooled samples having a distribution of diffusion domain sizes. *Journal of Geophysical Research*, *94*, 17,917–17,935. https://doi.org/10.1007/BF00286929

Ludwig, K. J. (2008). Isoplot 3.70. Berkeley Geochron. Center Spec. Publ., 4 (76 p.).
Lund, K., Beard, S. L., Blank, H. R. Jr., Hofstra, A. H., & Hamilton, M. M. (1988). Mineral resources of the Riordans Well Wilderness Study Area, Nye County, Nevada. USGS Bull., 1731-H (16 p.).
Lund, K., Beard, S. L., & Colgan, J. P. (2014). Shrimp U–Pb dating of zircon reveals Oligocene, Late Cretaceous, and Late Jurassic ages in Troy granite, east-central Nevada. Geol. Soc. Amer. Abstr. Prog., 46, 30.
Lund, K., Beard, S. L., & Perry, W. J. (1993). Relation between extensional geometry of the northern Grant Range and oil occurrences in Railroad Valley, east-central Nevada. *American Association of Petroleum Geologists Bulletin*, *77*, 45–962. https://doi.org/10.1306/BDFF8DA8-1718-11D7-8645000102C1865D
Lund, K., Nash, J. T., Beard, S. L., Blank, H. R. Jr., & Tuftin, S. E. (1987). Mineral resources of the Blue Eagle Wilderness Study Area, Nye County, Nevada. USGS Bull., 1731-D (19 p.).
McDowell, F. W., McIntosh, W. C., & Farley, K. A. (2005). A precise 40Ar/39Ar reference age for the Durango apatite (U–Th)/He and fission-track dating standard. *Chemical Geology*, *214*, 249–263.
McGrew, A. J., Peters, M. T., & Wright, J. E. (2000). Thermobarometric constraints on the tectonothermal evolution of the East Humboldt Range metamorphic core complex, Nevada. *Geological Society of America Bulletin*, *112*, 45–60. https://doi.org/10.1130/0016-7606(2000)112 < 45:TCOTTE>2.0.CO;2
McQuarrie, N., & Wernicke, B. P. (2005). An animated tectonic reconstruction of southwestern North America since 36 Ma. *Geosphere*, *1*, 147–172. https://doi.org/10.1130/GES00016.1
Miller, E. L., Dumitru, T. A., Brown, R. W., & Gans, P. B. (1999). Rapid Miocene slip on the Snake Range–Deep Creek Range fault system, east-central Nevada. *Geological Society of America Bulletin*, *111*, 886–905.
Miller, E. L., Gans, P. B., & Garing, J. (1983). The Snake Range décollement: An exhumed mid-Tertiary ductile-brittle transition. *Tectonics*, *2*, 239–263.
Min, K., Mundil, R., Renne, P. R., & Ludwig, K. R. (2000). A test for systematic errors in 40Ar/39Ar geochronology through comparison with U–Pb analysis of a 1.1 Ga rhyolite. *Geochimica et Cosmochimica Acta*, *64*, 73–98.
Molnar, P., & Lyon-Caen, H. (1988). Some simple aspects of the support, structure and evolution of mountain belts. In S. P. Clark, Jr., et al. (Eds.), *Processes in continental lithosphere deformation*, *Geol. Soc. Amer. Spec. Paper* (Vol. 218, pp. 179–207). Boulder, CO: Geological Society of America.
Moores, E. M., Scott, R. B., & Lumsden, W. W. (1968). Tertiary tectonics of the White Pine-Grant Range, east-central Nevada, and some regional implications. *Geological Society of America Bulletin*, *79*, 1703–1726.
Nicol, A., Walsh, J. J., Watterson, J., & Underhill, J. R. (1997). Displacement rates of normal faults. *Nature*, *390*, 157–159.
Orme, D. A., Reiners, P. W., Hourigan, J. K., & Carrapa, B. (2015). Effects of inherited cores and magmatic overgrowths on zircon (U-Th)/He ages and age-eU trends from Greater Himalayan sequence rocks, Mount Everest region, Tibet. *Geochemistry, Geophysics, Geosystems*, *16*, 2499–2507. https://doi.org/10.1002/2015GC005818
Potter, C. J., Dubiel, R. F., Snee, L. W., & Good, S. C. (1995). Eocene extension of early Eocene lacustrine strata in a complexly deformed Sevier-Laramide hinterland, northwest Utah and northeast Nevada. *Geology*, *23*, 181–184.
Quidelleur, X., Grove, M., Lovera, O. M., Harrison, T. M., Yin, A., & Ryerson, F. J. (1997). The thermal evolution and slip history of the Renbu Zedong Thrust, southeastern Tibet. *Journal of Geophysical Research*, *102*, 2659–2679. https://doi.org/10.1029/96JB02483
Quinlivan, W. D., & Rogers, C. L. (1974). Geologic map of the Tybo quadrangle, Nye County, Nevada. U.S.G.S. Misc. Invest. Map I-821.
Rahn, M. K., Brandon, M. T., Batt, G. E., & Garver, J. I. (2004). A zero-damage model for fission-track annealing in zircon. *American Mineralogist*, *89*, 473–484.
Reiners, P. W. (2005). Zircon (U-Th)/He thermochronometry. *Reviews in Mineralogy and Geochemistry*, *58*, 151–179. https://doi.org/10.2138/rmg.2005.58.6
Reiners, P. W., & Brandon, M. T. (2006). Using thermochronology to understand orogenic erosion. *Annual Review of Earth and Planetary Sciences*, *34*, 419–466. https://doi.org/10.1146/annurev.earth.34.031405.125202
Reiners, P. W., Spell, T. L., Nicolescu, S., & Zanetti, K. A. (2004). Zircon (U-Th)/He thermochronometry: He diffusion and comparisons with $^{40}Ar/^{39}Ar$ dating. *Geochimica et Cosmochimica Acta*, *68*, 1857–1887.
Rey, P. F., Teyssier, C., & Whitney, D. L. (2009). The role of partial melting and extensional strain rates in the development of metamorphic core complexes. *Tectonophysics*, *477*, 135–144.
Saleeby, J. (1993). Segmentation of the Laramide slab—Evidence from the southern Sierra Nevada region. *Geological Society of America Bulletin*, *115*, 655–668. https://doi.org/10.1130/0016-7606(2003)115 < 0655:SOTLSF>2.0.CO;2
Sanders, R. E., Heizler, M. T., & Goodwin, L. B. (2006). 40Ar/39Ar thermochronology constraints on the timing of Proterozoic basement exhumation and fault ancestry, southern Sangre de Cristo Range, New Mexico. *Geological Society of America Bulletin*, *118*, 1489–1506.
Schmitz, M. D., & Bowring, S. A. (2001). U–Pb zircon and titanite systematics of the Fish Canyon Tuff: An assessment of high-precision U–Pb geochronology and its application to young volcanic rocks. *Geochimica et Cosmochimica Acta*, *65*, 2571–2587. https://doi.org/10.1016/S0016-7037(01)00616-0
Scott, R. B. (1965). The Tertiary geology and ignimbrite petrology of the Grant Range, east-central Nevada (PhD dissertation, pp. 116). Houston, TX: Rice University.
Seedorff, C. E. (1991a). Royston district, western Nevada—A Mesozoic porphyry copper system that was tilted and dismembered by Tertiary normal faults. In G. L. Raines, R. E. Lisle, R. W. Schafer, & W. H. Wilkinson (Eds.), *Geology and ore deposits of the Great Basin* (pp. 359–391). Reno, NV: Geol. Soc. Nevada and U.S.G.S., Sympos. Proc.
Seedorff, E. (1991b). Magmatism, extension, and ore deposits of Eocene to Holocene age in the Great Basin—Mutual effects and preliminary proposed genetic relationships. In G. L. Raines, R. E. Lisle, R. W. Schafer, & W. H. Wilkinson (Eds.), *Geology and ore deposits of the Great Basin* (pp. 133–178). Reno, NV: Geol. Soc. Nevada Sympos. Proc.
Shaver, S. A., & McWilliams, M. (1987). Cenozoic extension and tilting recorded in Upper Cretaceous and Tertiary rocks at the Hall molybdenum deposit, northern San Antonio Mountains, Nevada. *Geological Society of America Bulletin*, *99*, 341–353.
Shuster, D. L., Flowers, R. M., & Farley, K. A. (2006). The influence of natural radiation damage on helium diffusion kinetics in apatite. *Earth and Planetary Science Letters*, *249*, 148–161.
Smith, D. L. (1992). History and kinematics of Cenozoic extension in the northen Toiyabe Range, Lander County, Nevada. *Geological Society of America Bulletin*, *104*, 789–801.
Snyder, R. P., Ekren, E. B., & Dixon, G. L. (1972). Geologic map of the Lunar Crater quadrangle, Nye County, Nevada. USGS Misc. Geol. Invest. Map I-700.

Sonder, L. J., England, P. C., Wernicke, B. P., & Christiansen, R. L. (1987). A physical model for Cenozoic extension of western North America. In M. P. Coward, J. F. Dewey, & P. L. Hancock (Eds.), *Continental extensional tectonics*, *Spec. Publ.* (Vol. 28, pp. 187–201). London: Geological Society.

Sonder, L. J., & Jones, C. H. (1999). Western United States extension: How the West was widened. *Annual Review of Earth and Planetary Sciences*, *27*, 417–462.

Speed, R. C., & McKee, E. H. (1976). Age and origin of the Darrough Felsite, southern Toiyabe Range, Nevada. *Journal of Research of the U.S. Geological Survey*, *4*, 75–81.

Spencer, J. E., & Reynolds, S. J. (1991). Tectonics of mid-Tertiary extension along a transect through west-central Arizona. *Tectonics*, *10*, 1204–1221. https://doi.org/10.1029/91TC01160

Steiger, R. H., & Jäger, E. (1977). Subcommission on geochronology: Convention on the use of decay constants in geo- and cosmochronology. *Earth and Planetary Science Letters*, *36*, 359–362.

Stewart, J. H. (1980). Geology of Nevada: A discussion to accompany the geologic map of Nevada. Nev. Bur. Mines Geol. Spec. Publ., 4 (136 pp.).

Stockli, D. F. (1999). Regional timing and spatial distribution of Miocene extension in the northern Basin and Range province (PhD thesis, pp. 239). Palo Alto, CA: Stanford University.

Suppe, J. (1983). Geometry and kinematics of fault-bend folding. *American Journal of Science*, *283*, 684–721. https://doi.org/10.2475/ajs.283.7.684

Suppe, J., & Medwedeff, D. A. (1990). Geometry and kinematics of fault-propagation folding. *Eclogue Geologicae Helvetica*, *83*, 409–454.

Taylor, J. R. (1982). *An introduction to error analysis: The study of uncertainties in physical measurements* (p. 270). Mill Valley, CA: University Science Books.

Taylor, W. J. (1990). Magnitude and temporal relations of episodic Cenozoic extension in the North Pahroc and Seaman Ranges, Nevada. In B. P. Wernicke (Ed.), *Tertiary extensional tectonics near the latitude of Las Vegas*, *Geol. Soc. Amer. Mem.* (Vol. 176, pp. 181–193). Boulder, CO: Geological Society of America.

Taylor, W. J., & Bartley, J. M. (1992). Prevolcanic extensional Seaman breakaway fault and its geologic implications for eastern Nevada and western Utah. *Geological Society of America Bulletin*, *104*, 255–266.

Taylor, W. J., Bartley, J. M., Lux, D. R., & Axen, G. J. (1989). Timing of Tertiary extension in the Railroad Valley-Pioche transect, Nevada: Constraints from $^{40}Ar/^{39}Ar$ ages of volcanic rocks. *Journal of Geophysical Research*, *94*, 7757–7774. https://doi.org/10.1029/JB094iB06p07757

Taylor, W. J., Bartley, J. M., Martin, M. W., Geissman, J. W., Walker, J. D., Armstrong, P. A., & Fryxell, J. E. (2000). Relations between hinterland and foreland shortening: Sevier orogeny, central North American Cordillera. *Tectonics*, *19*, 1124–1143. https://doi.org/10.1029/1999TC001141

Wells, M. L., & Hoisch, T. D. (2008). The role of mantle delamination in widespread Late Cretaceous extension and magmatism in the Cordilleran orogen, western United States. *Geological Society of America Bulletin*, *120*, 515–530. https://doi.org/10.1130/B26006.1

Wells, M. L., Hoisch, T. D., Cruz-Aribe, A. M., & Vervoort, J. D. (2012). Geodynamics of synconvergent extension and tectonic mode switching: Constraints from the Sevier-Laramide orogeny. *Tectonics*, *31*, TC1002. https://doi.org/10.1029/2011TC002913

Wells, M. L., Snee, L. W., & Blythe, A. E. (2000). Dating of major normal fault systems using thermochronology: an example from the Raft River detachment, Basin and Range, western United States. *Journal of Geophysical Research*, *105*, 16,303–16,327.

West, D. P., & Lux, D. R. (1993). Dating mylonitic deformation by the $^{40}Ar/^{39}Ar$ method: An example from the Norumbega fault zone, Maine. *Earth and Planetary Science Letters*, *120*, 221–237.

Yamada, R., Murakami, M., & Tagami, T. (2007). Statistical modeling of annealing kinetics of fission tracks in zircon: Reassessment of laboratory experiments. *Chemical Geology*, *236*, 75–91.

Yonkee, W. A., & Weil, A. B. (2015). Tectonic evolution of the Sevier and Laramide belts within the North American Cordillera orogenic system. *Earth-Science Reviews*, *150*, 531–593. https://doi.org/10.1016/j.earscirev.2015.08.001